Activity-based probes and chemical proteomics uncover the biological impact of targeting HMGCS1.

Sang Ah Yi[1,‡], Liang Sun[1,‡], Yi Rao[2,3,4], Alban Ordureau[5], Jason S. Lewis[2,3,4], and Heeseon An[1,4*]

[1]Chemical Biology Program, Sloan Kettering Institute, Memorial Sloan Kettering Cancer Center, New York, NY, USA

[2]Department of Radiology, Memorial Sloan Kettering Cancer Center, New York, NY, USA.

[3]Molecular Pharmacology Program, Sloan Kettering Institute, Memorial Sloan Kettering Cancer Center, New York, NY, USA.

[4]Department of Pharmacology, Weill Cornell Graduate School of Medical Sciences, New York, NY, USA

[5]Cell Biology Program, Sloan Kettering Institute, Memorial Sloan Kettering Cancer Center, New York, NY, USA

[‡]These authors contributed equally

*Corresponding author: anh@mskcc.org

ABSTRACT

Mevalonate is a precursor for essential metabolites, such as isoprenoids and sterols. Its synthesis starts with HMGCS1 producing HMG-CoA, which is then converted to mevalonate by HMGCR, a target of statins. Cancer cells often upregulate enzymes in the mevalonate pathway (MVP) to meet their metabolic demands, leading to the development of inhibitors targeting several enzymes in this pathway. However, current inhibitors have not yet shown significant anti-cancer activity. While HMGCS1 has unique biochemical properties that distinguish it from other MVP enzymes, the effects of inhibiting HMGCS1 have not been thoroughly investigated. Here, we present a set of chemical probes that enable us to systematically assess the proteome-wide selectivity and potency of Hymeglusin, the primary inhibitor of HMGCS1 used in the field, confirming it as a useful tool for short-term HMGCS1 inhibition. Inhibiting HMGCS1 with Hymeglusin causes proteome changes that are nearly identical to those caused by inhibiting HMGCR or degrading HMGCS1. Accordingly, simultaneously targeting HMGCS1 and HMGCR effectively suppresses the growth of statin-resistant cells and xenograft models, without increasing the risk of side effects. Finally, we find that while Hymeglusin is a valuable tool for short-term mechanistic studies, its usefulness is limited for long-term efficacy studies due to its poor stability in serum. Together, this study highlights the biological implications of targeting HMGCS1 as monotherapy or in combination with statins, and caution is required when using Hymeglusin as a tool.

KEYWORDS

HMGCS1, Mevalonate, Hymeglusin, HMGCR, statin, chemical proteomics, activity-based probe

53 **INTRODUCTION**

54 Mevalonate is an essential precursor for the biosynthesis of sterols, isoprenoids, vitamin D, and
55 ubiquinone.(1, 2) Consequently, the enzymes involved in the mevalonate pathway (MVP) play
56 crucial roles in multiple aspects of cellular physiology, from membrane biology to cell signaling
57 and mitochondrial metabolism.(3) The synthesis of mevalonate begins with the first step,
58 catalyzed by 3-Hydroxy-3-Methylglutaryl-Coenzyme A Synthase 1 (HMGCS1), which condenses
59 acetyl-CoA with acetoacetyl-CoA to produce HMG-CoA. The HMG-CoA then undergoes
60 reduction to mevalonate via HMG-CoA Reductase (HMGCR). Following this, approximately 20
61 downstream enzymes convert mevalonate into sterols and other non-sterol end-products.
62 Growing evidence indicates that cancer cells exhibit upregulation of MVP enzymes, which may
63 stimulate glucose uptake and various signaling pathways, including RAS, RAB, and RHO.(4-8)
64 This upregulation has also been linked to resistance to various chemotherapies, emphasizing the
65 significance of these enzymes in cancer progression and their ability to manage stress.(9-11)
66 Prior research suggests that inhibiting the mevalonate pathway induces apoptotic death of cancer
67 cells by blocking the geranylgeranylation of proteins.(12, 13) Consequently, several enzymes in
68 this pathway, such as HMGCR, FDPS, GGDPS1, FTase, and GGTase, have been exploited as
69 potential pharmacological targets.(5, 7) However, the existing approaches or inhibitors have yet
70 to produce significant clinical anti-cancer activity.(7, 14-21)
71
72 HMGCS1 represents an underexplored pharmacological target within the mevalonate pathway,
73 despite the fact that it possesses several attractive features that distinguish it from HMGCR and
74 other downstream MVP enzymes. Notably, HMGCS1 contains a catalytic cysteine in its active
75 site that can be readily leveraged for developing covalent inhibitors and chemical probes to
76 enhance potency and sustained efficacy compared to non-covalent inhibitors. Moreover, we
77 previously demonstrated that HMGCS1 levels are directly regulated by the master regulator of
78 cell growth, mTORC1,(22) and an increased requirement for HMGCS1 during the activation of
79 cell proliferation signals makes it a limiting enzyme in cells with hyperactive mTORC1, a frequently
80 observed feature of cancer cells. Thus, perturbation of HMGCS1 can be an alternative strategy
81 to treat cancers exhibiting upregulated metabolites and signaling pathways related to MVP. (22)
82
83 However, the chemical tools available to perturb the HMGCS1 activity are currently limited, with
84 Hymeglusin serving as the primary small molecule probe.(10, 23, 24) Identified as an HMGCS1
85 inhibitor in 1987, Hymeglusin was isolated from Fusarium and Scopulariopsis fungi.(25-30) The

86 co-crystal structure of HMGCS1 and Hymeglusin revealed that Hymeglusin forms a thioester bond
87 with the catalytic cysteine of HMGCS1 following the opening of its lactone ring.(31) A subsequent
88 study showed that this HMGCS1-Hymeglusin adduct is stable *in vitro*, with an estimated half-life
89 of 55 hours.(26) The same study also showed that Hymeglusin-mediated inhibition of HMGCS1
90 in cells is reversed within 30 minutes after withdrawal when measured by the conversion of
91 radioactive acetate into cholesterol.(26) However, the occupancy level of the intracellular
92 HMGCS1 catalytic cysteine and the cause of this increased reversibility of Hymeglusin remain
93 unclear, primarily due to the lack of tools that allow direct monitoring. Additionally, a
94 comprehensive quantitative analysis of the reactivity of Hymeglusin toward the global proteome,
95 as well as its effects on reshaping the proteome landscape, has not been reported.
96
97 In the present study, we have developed activity-based probes for HMGCS1, functionalized with
98 fluorescent dye or biotin handles, that facilitate the investigation of the effects of covalent inhibition
99 of HMGCS1 in human cells. By combining these probes with proteomics analyses, we show that
100 Hymeglusin specifically reacts with the catalytic cysteine of HMGCS1 in cells. Hymeglusin
101 treatment induces global proteomic changes that are nearly identical to those induced by the
102 HMGCR inhibitor, Simvastatin. Our unbiased data support the selective inhibition of mevalonate
103 synthesis by Hymeglusin and reveal non-redundant functions of HMGCS1 and HMGCR outside
104 the mevalonate pathway. Consequently, the concurrent targeting of both enzymes potentiates
105 inhibition of mevalonate synthesis, leading to increased anti-cancer effects in cells and in mouse
106 xenograft models. We also demonstrate that targeted proteolysis of HMGCS1 exhibits a more
107 potent anti-proliferation effect than inhibition by Hymeglusin, due to its poor serum stability. In
108 conclusion, this study presents a comprehensive toolkit for inhibiting and analyzing HMGCS1
109 activity, providing insights into the cellular and pharmacological effects of this intervention.

110 **RESULTS**

111 **Hymeglusin-fluorescence conjugates monitor occupancy of the HMGCS1 active site.**
112 HMGCS1 is a 57 kDa protein known to form tight homodimers in cells and *in vitro*.(22, 32) A
113 previous co-crystal structure showed that Hymeglusin forms a covalent bond with the catalytic
114 cysteine of HMGCS1, thereby inhibiting its enzymatic activity (**Fig. 1A**).(33) While Hymeglusin
115 has been used as a representative inhibitor of HMGCS1 for biological studies,(10, 23, 24) its
116 proteome-wide selectivity has not been evaluated quantitatively. This lack of comprehensive
117 evaluation creates uncertainties about its biological implications and on-target effects. We,
118 therefore, synthesized fluorescent probes by conjugating the Hymeglusin warhead to two different

119 dyes, fluorescein or tetramethylrhodamine (TMR), through a linker (**Fig. 1B**). The Hymeglusin-
120 fluorecein (HG-FL) probe was then incubated with either wild-type (WT) or a catalytically inactive
121 HMGCS1 harboring a Cys-Ala substitution *in vitro*, after purifying them from HEK293T cells (**Fig.**
122 **1C**). In-gel fluorescence analysis showed a signal exclusively in wild-type HMGCS1, indicating
123 that HG-FL binds the catalytic cysteine residue. When recombinant HMGCS1 was pre-treated in
124 vitro with different concentrations of Hymeglusin before adding HG-FL, the fluorescent signal
125 decreased in a dose-dependent manner (**Fig. 1D**). HG-FL binding to HMGCS1 was disrupted in
126 the presence of a reducing agent, dithiothreitol (DTT), which may cleave the thioester bond
127 formed between Cys129 and Hymeglusin (**Fig. 1E**). However, the strong resistance of this
128 interaction under denaturing conditions implied a tight binding of Hymeglusin to the hydrophobic
129 pocket, which hinders the access of DTT for trans thiolation reaction. We subsequently
130 investigated whether HG-fluorescence probes could be used to monitor the occupancy of the
131 catalytic cysteine residue within intracellular HMGCS1 (**Fig. 1F,** upper panel). WT HEK293T cells
132 were treated with Hymeglusin for 2 hours, followed by cell lysis, and incubation with the HG
133 probes. Subsequent in-gel fluorescence analyses revealed a fluorescence band that was
134 reversed upon pre-incubation of cells with Hymeglusin (**Fig. 1F**, bottom left panel). CRISPR-
135 engineered HCT116 cells expressing endogenous HMGCS1-FKBP12^{F36V} or HMGCS1-mEGFP
136 fusion protein showed similar results when probed by either HG-FL or HG-TMR, with the shifts in
137 molecular weight that match with HMGCS1 chimera (**Fig. 1F**, bottom middle/right panels). The
138 same gels were then subjected to immunoblotting for HMGCS1 detection, and the fluorescent
139 bands coincided with the bands detected by the anti-HMGCS1 antibody. These data indicate that
140 HG-fluorescence probes can serve as activity-based probes for HMGCS1.
141

142 Does Hymeglusin occupancy of the HMGCS1 catalytic cysteine lead to the depletion of cellular
143 HMG-CoA, the product of HMGCS1 enzymatic activity? Previous investigations have
144 demonstrated that the accumulation of HMG-CoA in cells, resulting from the inhibition of HMGCR
145 by statins, facilitates a non-enzymatic reaction with fatty acid synthase (FASN), leading to the
146 formation of HMG-modified FASN (**Fig. 1G,** upper panel).(34) The presence of this modification
147 can be effectively monitored using an anti-HMG antibody.(35) Notably, prior studies have shown
148 that the overall reactivity of this antibody correlates with intracellular levels of HMG-CoA. Indeed,
149 when HCT116 cells expressing endogenous HMGCS1-FKBP12^{F36V} fusion protein were treated
150 with Simvastatin, an HMG positive band appeared around 240 kDa range (**Fig. 1G**, bottom panel,
151 first two lanes). The addition of the dTAGv1 ligand, which recruits the VHL-containing E3 ligase
152 complex to the FKBP12^{F36V} tag and induces the degradation of HMGCS1-FKBP12^{F36V}chimera,

153 caused the disappearance of the HMGylated protein signal (**Fig. 1G,** bottom panel, third lane,
154 and **Fig. S1A**).(22, 36) This indicates that the cellular HMG-CoA level dropped in the absence of
155 HMGCS1, serving as the positive control for this assay system. Treatment with increasing
156 concentrations of Hymeglusin similarly led to a progressive decrease in the HMGylated protein
157 intensity, indicating inhibition of HMGCS1 activity. Of note, statin treatment induced a substantial
158 increase in HMGCS1 and HMGCR levels due to the feedback effect mediated by the SREBP2
159 transcription factor.(37)

160

161 **Hymeglusin reacts highly selectively with HMGCS1 in human cells.**

162 We next evaluated the reactivity of Hymeglusin toward the human proteome using an unbiased
163 chemical proteomics approach. To conclusively identify the Hymeglusin-labeled proteins using
164 mass spectrometry, we synthesized the Hymeglusin-biotin (HG-Biotin) probe (**Fig. 2A**, top).
165 HEK293T cells were either treated with Hymeglusin or DMSO for 30 min prior to incubation with
166 HG-biotin. The proteins labeled with HG-biotin were enriched using streptavidin beads, and the
167 eluates were analyzed using a 6-plex tandem-mass-tag (TMT)-based quantification. Our
168 proteomic analysis revealed that HMGCS1 is the only significantly enriched protein that was
169 displaced by the pretreatment with Hymeglusin (12-fold increase, 50 peptides detected),
170 demonstrating Hymeglusin's high selectivity for HMGCS1 (**Fig. 2B**). An orthogonal
171 immunoblotting assay confirmed the strong enrichment of HMGCS1 by HG-biotin (**Fig. 2C**). In
172 contrast, endogenously biotinylated proteins such as ACACA (18 peptides), PCCA (19 peptides),
173 and MCCC1 (14 peptides), were enriched regardless of Hymeglusin pre-treatment, as a
174 consequence of their interaction with streptavidin (**Table S1**). Consistently, the HG-FL assay on
175 HEK293T cells that were pretreated with increasing concentrations of Hymeglusin revealed a
176 single strong fluorescence signal around 57 kDa, corresponding to the molecular weight of
177 HMGCS1 (**Fig. 2D**). This signal disappeared when the cells were pretreated with 250-500 nM
178 Hymeglusin. We conclude that Hymeglusin is a potent and selective inhibitor of HMGCS1, making
179 it a suitable tool for examining the downstream biological effects of acute HMGCS1 inhibition.

180

181 **The inhibition or degradation of HMGCS1, or inhibition of HMGCR, results in identical**
182 **changes to the proteome.**

183 To gain a deeper understanding of the cellular response to the inhibition of HMGCS1, we analyzed
184 global proteomic changes following Hymeglusin treatment (**Fig. 3A**, left). We compared the
185 proteome alterations caused by the acute degradation of HMGCS1 by using the HCT116
186 HMGCS1-FKBP12^{F36V} knock-in cells, which may decouple any side effects of Hymeglusin and

187 non-enzymatic roles of HMGCS1, if they exist. We also compared the proteome changes induced
188 by the inhibition of HMGCR, as HMGCS1 and HMGCR are the first two enzymes in the
189 mevalonate pathway (**Table S2**). If these two enzymes have additional functions outside the
190 mevalonate pathway, it may be evident in the proteome changes. Immunoblotting analysis
191 showed that dTAGv1 treatment for 24 hours led to the expected depletion of HMGCS1 and the
192 upregulation of unprenylated RhoA and HMGCR, a known feedback effect (**Fig. 3A**, right).(38)
193 Hymeglusin treatment also resulted in an increase of RhoA and HMGCR, along with HMGCS1.
194 Similarly, statin treatment caused a significant increase in RhoA, HMGCR, and the emergence of
195 HMGylated FASN. These data suggest that each condition results in a comparable degree of
196 mevalonate flux perturbation. Accordingly, the TMT-based proteomics approach was applied to
197 the cells under the corresponding conditions in four replicates, and the overall quality of the
198 samples was assessed again through immunoblotting (**Fig. 3B,C**). The following mass-
199 spectrometry analysis revealed the relative abundance of 9,881 proteins across all 16 samples
200 without missing values. Principal component analysis showed that replicates of each sample
201 clustered together, indicating consistency among the replicates (**Fig. S2A**). Notably, only the
202 untreated cells showed a distinct separation, while the cells treated with the mevalonate pathway
203 inhibition formed a closely clustered group. For example, proteome profiles from cells treated with
204 Simvastatin and Hymeglusin showed nearly identical results, indicated by a strong Pearson
205 correlation coefficient of 0.97 (**Fig. S2B**). A similarly high correlation coefficient (Pearson r = 0.95)
206 was observed when comparing Hymeglusin-treated cells with those subjected to HMGCS1
207 degradation (**Fig. S2C**). These unbiased proteomics data reveal that 1) Hymeglusin produces
208 proteome changes that are highly specific to HMGCS1 inhibition, 2) HMGCS1 depletion causes
209 proteome changes driven by the loss of its enzymatic function, and 3) targeting HMGCS1 and
210 HMGCR leads to the nearly identical proteomic changes in 24 hours, reinforcing their essential
211 role in the mevalonate pathway.
212
213 12% of the total proteome (1,200 of 9,881 proteins) showed significant changes within 24 hours
214 of Hymeglusin treatment. It was evident that the inhibition of the mevalonate pathway substantially
215 stimulated the production of a subset of the proteome, with 168 proteins increasing by more than
216 two-fold while 24 proteins decreased (**Fig. 3D**). Gene Ontology (GO) analysis of the significantly
217 upregulated proteins (> 2-fold, 168 proteins) for their cellular compartment indicated that the
218 proteins in the secretory pathway are significantly enriched (**Fig. 3E**). Functionally, proteins
219 involved in regulating cell migration and signaling receptor binding were prominent (30 and 38
220 proteins, respectively), aligning with the role of the mevalonate pathway in regulating small

221 GTPase family members, such as RHO, RAB, and RAS. A notable increase was also observed
222 in ~ 20 enzymes within the mevalonate pathway across the various treatment conditions (**Fig.**
223 **3F**). All three inhibitory conditions resulted in a similar induction of the mevalonate pathway
224 enzymes. These findings are consistent with prior reports of a transcriptional feedback
225 mechanism mediated by Sterol Regulatory Element-Binding Protein 2, which is triggered upon
226 the inhibition of MVP enzymes.(39) Significantly downregulated proteins (greater than 2-fold
227 difference, 24 proteins) included seven proteins involved in the mitotic spindle checkpoint,
228 indicating that cell cycle arrest was initiated, likely as a sign of early-stage apoptosis (**Fig. 3D**). In
229 this context, BCL2L12, an anti-apoptotic regulator, was downregulated by more than 2-fold.
230 Mevalonate is a precursor for not only sterols but also isoprenoids that are essential for post-
231 translational modifications, such as farnesylation and geranylgeranylation. Three proteins
232 targeted by farnesylation (RAB20, RAB29, RAB12) and two proteins for geranylgeranylation with
233 a CAAX motif (MIEN1 and FBXO10) were significantly downregulated, suggesting their
234 destabilization due to the loss of prenylation. When we examined the changes in prenylation
235 substrates on a broader scale, we found many of them among the statistically significant hits.
236 Intriguingly, they showed divergent expression changes upon the inhibition of mevalonate
237 production (**Fig. 3G**). Their downregulation may stem from instability caused by the lack of
238 prenylation in the newly produced proteins, while the up-regulated proteins may be a result of
239 their transcriptional feedback effect mediated by SREBP2, producing unprenylated RHO and RAB
240 proteins. In any case, their cellular functions may be negatively affected by the loss of prenylation.
241 In summary, the inhibition or degradation of HMGCS1, or the inhibition of HMGCR by statins,
242 results in a similar alteration of the global proteome that is characterized by the induction of the
243 MVP enzymes and the substrates of the downstream metabolites, isoprenoids.
244
245 **Simultaneous targeting HMGCS1 and HMGCR produces a synergistic anti-cancer**
246 **response**.
247 Repurposing statins has attracted significant interest as a strategy for treating cancer.(20)
248 However, many patients were non-responsive to statin treatment. Prior studies have suggested
249 that cells demonstrating feedback upregulation of the MVP enzymes, particularly HMGCS1, tend
250 to exhibit strong statin resistance.(40-42) We tested this by using seven cell lines with different
251 lineages. Simvastatin treatment for 24 hours led to varying levels of HMGCS1 induction (**Fig.**
252 **S3A, B**). Among the seven cell lines, HCT116 showed a 2.5-fold increase in HMGCS1, while the
253 HMGCS1 levels in HEK293T or MFE296 cell lines remained unaltered (**Fig. S3C**). The following
254 cell viability assay on HCT116 and HEK293T cells indicated that HCT116 cells are highly resistant

255 to Simvastatin treatment, while HEK293T cells were relatively more sensitive (**Fig. S3D**). Colony
256 formation assays on HCT116 and MFE296 cells also showed resistance for HCT116, whereas
257 MFE296 cells exhibited a more sensitive response (**Fig. S3E**). Based on our data and the prior
258 study, we conclude that the increased production of HMGCS1 upon statin treatment may
259 contribute to the low efficacy of statins in HCT116.
260
261 The strong correlation observed between changes in the global proteome caused by the inhibition
262 of HMGCS1 and HMGCR suggests that simultaneously targeting both enzymes may more
263 effectively inhibit the mevalonate metabolic pathway. This could address the current limitation of
264 statin efficacy in anti-cancer therapy, especially in cells that are resistant to statins. We, therefore,
265 examined if simultaneous targeting of HMGCS1 and HMGCR would enhance the anti-proliferative
266 effect of the monotherapy using HCT116 cells (**Fig. 4A**). In a colony formation assay, treatment
267 with a statin alone resulted in a ~30% decrease in the number of colonies, while Hymeglusin
268 alone had a negligible effect. In contrast, combined treatment with Symvastatin and Hymeglusin
269 resulted in significant inhibition of colony formation. Similarly, we examined the effect of HMGCS1
270 degradation on cell proliferation, both individually and in combination with a statin, using HCT116
271 cells expressing endogenous HMGCS1-FKBP12^{F36V} fusion protein (**Fig. 4B**). In these cells,
272 Simvastatin treatment resulted in a substantial increase in endogenous HMGCS1-FKBP12^{F36V},
273 as expected, whereas addition of dTAGv1 nearly depleted HMGCS1 via induced degradation.
274 Treatment of dTAGv1 in these cells led to a 60% reduction in colony numbers, while co-treatment
275 with dTAGv1 and Simvastatin resulted in nearly complete inhibition of colony formation (**Fig.**
276 **4C,D)**. Similarly, cell viability assay results gained from the monolayered cell culture system
277 indicated that the addition of dTAGv1 ligand significantly enhanced the IC_{50} of Simvastatin,
278 decreasing from 15.6 μM to 1.3 μM (**Fig. 4E**). As a control, we treated wild-type HCT116 cells
279 with the dTAGv1 ligand, which exhibited no change in the IC_{50} of Simvastatin, confirming that the
280 observed change in IC_{50} was due to the degradation of HMGCS1 (**Fig. 4E,** bottom). Importantly,
281 the cell death caused by the joint treatment was rescued by supplementing the media with
282 geranylgeranyl alcohol (GGOH), a precursor of the downstream metabolite of the mevalonate,
283 indicating that the enhanced cytotoxicity arises from the impairment of the mevalonate synthesis
284 (**Fig. 4F**).
285
286 Lastly, we performed the equivalent study using the mouse xenograft model after implanting
287 HCT116 HMGCS1-FKBP12^{F36V} cells (**Fig. 4G,H**). Four groups of mice were subjected to two
288 treatment regimens over a two-week interval, including saline control, oral Simvastatin three times

289 a week, weekly i.p. injection of dTAGv1, and the combination of Simvastatin and dTAGv1. The
290 group of mice that received both Simvastatin and dTAGv1 exhibited a synergistic effect on tumor
291 growth suppression that lasted for 40 days. In contrast, administration of Simvastatin or dTAGv1
292 ligand injection alone did not show a significant difference compared to the PBS-treated control
293 group. Overall data suggest that dual targeting of HMGCS1 and HMGCR may offer potential
294 benefits, and the targeted proteolysis approach for HMGCS1 perturbation could demonstrate
295 greater efficacy compared to inhibition.
296
297 **Hymeglusin warhead exhibits poor serum stability.**

298 Despite identical proteome changes upon degradation or inhibition of HMGCS1 (**Fig. 3**),
299 enzymatic inhibition of HMGCS1 by Hymeglusin did not elicit any cytotoxic effects in either
300 HCT116 or HEK293T cells. when used alone (**Figs. 4A and S4A**). This observation is inconsistent
301 with the anti-tumor efficacy of dTAGv1-mediated HMGCS1 degradation, prompting us to further
302 investigate the long-term stability of Hymeglusin. Prior investigations using murine models
303 administered with Hymeglusin reported an 80% reduction in cholesterol synthesis within 30 min
304 and a complete loss of inhibitory function by 180 min when measured by the conversion of ^{14}C-
305 labeled acetate into plasma cholesterol.(25, 26) It was speculated that this effect may be due to
306 the reversible nature of the thioester bond formed between Hymeglusin and HMGCS1. However,
307 the precise kinetics underlying the decline in Hymeglusin efficacy and the mechanism behind its
308 loss of efficacy in cells remain to be determined. Considering that researchers have utilized
309 Hymeglusin as an inhibitor of HMGCS1 in a range of cell culture models, elucidating this limitation
310 could be crucial for its appropriate application. Our use of the HMGCS1 activity-based probes
311 enabled us to monitor the occupancy of the catalytic cysteine in HMGCS1 by Hymeglusin over
312 time. After 8 hours of treatment with 0.5 μM Hymeglusin, we observed the emergence of the
313 catalytically active HMGCS1 that was labeled with HG-FL, a trend that became more pronounced
314 after 16 hours in HEK293T, HCT116, or HepG2 cells (**Fig. 5A,B**). These data indicate that
315 HMGCS1 labeling is not maintained over the long term, which aligns with the absence of
316 sustained efficacy in the antiproliferative effects we observed with Hymeglusin treatment.
317 Interestingly, the removal of serum from the culture media led to a delayed restoration of active
318 HMGCS1 levels, indicating that serum plays a role in the short-term efficacy of Hymeglusin (**Fig.**
319 **5C**). Indeed, when Hymeglusin was pre-incubated in DMEM with 10% FBS for 16 hours before
320 being added to the cells, the catalytic cysteine of HMGCS1 was not effectively inhibited anymore
321 (**Fig. 5D,E**). In contrast, pre-incubation in DMEM without 10% FBS did not reduce the efficacy of
322 Hymeglusin. Additionally, we observed intense labeling of bovine serum albumin (BSA) by HG-

323 FL after incubating them for one hour *in vitro* (**Fig. 5F**). The labeling persisted even after boiling
324 for 5 minutes in denaturing conditions, suggesting a strong interaction between HG-FL and BSA.
325 We tried to clarify this by categorizing the potential pathways that underlie how BSA impacts the
326 efficacy of Hymeglusin into two distinct types: First, BSA contains 35 cysteines, of which 34 form
327 disulfide bonds, leaving one reactive cysteine.(43) Thus, Hymeglusin may form a covalent bond
328 with BSA via reactive Cys34. The second possibility is that Hymeglusin forms a non-covalent, yet
329 strong, interaction through the fatty acid binding sites, as BSA has several fatty acid binding sites
330 and Hymeglusin resembles the structure of fatty acids.(44) As the second possibility is rather
331 complex to address, we evaluated the first hypothesis. If the cysteine on the BSA is reacting with
332 HG-FL, then alkylating BSA with chloroacetamide prior to HG-FL incubation should result in no
333 labeling. We thus treated BSA with chloroacetamide, and the loss of reactive cysteine was
334 confirmed by using Ellman's reagent (**Fig. 5G, H**). When native BSA was incubated with Ellman's
335 reagent, the solution changed to yellow due to the formation of 2-nitro-5-thiobenzoate (TNB). After
336 pre-incubating the BSA with chloroacetamide, we observed the expected loss of color change,
337 representing the absence of active cysteine on BSA (**Fig. 5H**). Then, this alkylated BSA was
338 treated with HG-FL, with non-alkylated BSA serving as a positive control (**Fig. 5I**). The subsequent
339 in-gel fluorescence analysis revealed an unchanged fluorescence signal, suggesting that
340 hymeglusin likely binds to BSA through non-covalent interactions. Together, poor serum stability
341 may limit the long-term use of Hymeglusin in cell and in vivo studies, as human serum typically
342 contains ~ 40 mg/mL of albumin.

343

344 **DISCUSSION**

345 The mevalonate pathway is a well-established focus of interest for chemists and biologists, given
346 its critical role in cholesterol biogenesis and prenylation. Prenylation, in particular, is essential for
347 the proper function of several oncogenic proteins, such as RAS, which underscores its
348 contribution to cancer progression. Consequently, several enzymes in the mevalonate pathway
349 have received substantial attention in pharmaceutical research for inhibitor development.
350 However, the initial enzyme of the pathway, HMGCS1, has received relatively little focus,
351 overshadowed by HMGCR and the established use of statins. We have recently discovered that
352 HMGCS1 functions as a gatekeeper of this pathway, especially in cells with hyperactive mTORC1
353 signaling.(22) HMGCS1 senses and responds to fluctuations in mTORC1 activity, paralleling the
354 critical role of HMGCR in sensing and responding to changes in membrane sterol levels.

355 Moreover, the presence of a ligandable cysteine in HMGCS1 makes it a particularly unique and
356 advantageous target for probe development, which can significantly facilitate investigations into
357 both the mechanisms of inhibitor action and potential resistance.

358 Currently, few tools are available to interrogate HMGCS1. Among them, Hymeglusin, a natural
359 product derived from fungi, stands out as the primary tool utilized in the field since its discovery
360 in the 1980s.(25-29, 45) Despite its widespread use, the selectivity and overall efficacy of
361 Hymeglusin in cells have not been thoroughly evaluated since the 1990s, raising concerns about
362 its suitability as a tool compound. This prompted us to assess its cellular potency and selectivity
363 by developing activity-based probes inspired by the Hymeglusin warhead and leveraging modern
364 technologies, such as proteomics. Our unbiased analyses, grounded in chemical biology
365 approaches, revealed that Hymeglusin is a potent and highly selective inhibitor of HMGCS1 in
366 HEK293T cells, with a concentration of 0.5 μM fully saturating the catalytic cysteine of HMGCS1
367 in cells. However, we also determined that Hymeglusin has extremely poor serum stability,
368 apparently derived from the interaction with serum albumin, which is comparable to on-target
369 binding to HMGCS1. This drawback limits the duration and efficacy of Hymeglusin to target
370 HMGCS1. Nevertheless, our comprehensive data led us to consider Hymeglusin a viable tool for
371 studying the short-term pharmacologic effects of HMGCS1 inhibition, provided we carefully
372 monitor its intracellular stability and activity with our activity-based probes.

373 After carefully characterizing Hymeglusin, we explored the effect of inhibiting HMGCS1 using
374 Hymeglusin and an additional method that incorporates a chemical genomic approach to induce
375 the degradation of HMGCS1. Proteomic analysis of cells following HMGCS1 inhibition or
376 degradation, or HMGCR inhibition, revealed surprisingly similar proteome changes in 24 hours.
377 This result indicates that targeting both enzymes simultaneously may enhance drug efficacy
378 without amplifying the risk of potential side effects from either inhibitor. Our follow-up cell
379 biological and xenograft studies support this notion that dual targeting of HMGCS1 and HMGCR
380 potentiates the anti-cancer effect of statin monotherapy. Overall, our findings highlight the
381 potential of targeting HMGCS1 either as a monotherapy or in combination with statins,
382 emphasizing the benefits of the induced proteolysis approach in this context.

383 Comparative analysis of HMGCS1 inhibition by Hymeglusin or of HMGCS1 degradation using the
384 chemically induced tag system (dTAG) demonstrated the superior potency of the degradation
385 approach in inhibiting cancer cell proliferation. Heterobifunctional degrader molecules have
386 potential therapeutic advantages over the monofunctional inhibitor.(46, 47) In the case of

387 HMGCS1, the proteolysis targeting chimera (PROTAC) degrader can counteract the
388 compensatory upregulation of HMGCS1 through its degradation. As the half-life of the HMGCS1
389 protein spans several days, the drug-induced degradation of HMGCS1 can be prolonged longer
390 than the inhibitors. Additionally, covalent PROTACs have been shown to enhance cellular uptake
391 and target selectivity.(48) Therefore, developing small molecules that could induce targeted
392 proteolysis of HMGCS1 may offer better pharmacological properties than inhibitors, providing a
393 more effective strategy to treat cancer both as monotherapy and in combination with HMGCR
394 inhibitors.

395 Although we here defined that Hymeglusin interacts with albumin through non-covalent binding,
396 further investigation is needed to determine the detailed binding mode between Hymeglusin and
397 albumin protein.(49) One possibility is that the structure of Hymeglusin resembles that of fatty
398 acids. Albumin has well-characterized fatty acid binding pockets, with at least seven known
399 pockets that could potentially interact with Hymeglusin.(50) Another limitation of the present study
400 is that the mitochondrial HMG-CoA synthase, HMGCS2, which shares approximately 60%
401 sequence identity with HMGCS1, may be another potential target of Hymeglusin. HMGCS2
402 exhibits tissue-specific expression profiles, unlike the universal expression of HMGCS1.
403 Therefore, this aspect should be considered when using Hymeglusin for cell lines that express
404 HMGCS2.

405 In summary, this study reports new chemical biology tools for an important yet underexplored
406 metabolic enzyme within cells, HMGCS1. It offers insights into how targeting HMGCS1—either
407 alone or together with HMGCR—can lead to alterations in the identical cellular proteome while
408 potentiating their anti-proliferation effect. Furthermore, the study holds potential for developing
409 drug-like inhibitors or bisubstrate degraders of HMGCS1 by utilizing the activity-based probes
410 developed in this study.

411

412 **EXPERIMENTAL PROCEDURES**

413 Detailed information about reagents and resources used in this study are displayed in Table S3.

414

415 **Cell culture**

416 HEK293T, HCT116, RPE1, HeLa, and HepG2 cells were grown in Dulbecco's modified Eagle's
417 medium (DMEM), supplemented with 10% fetal bovine serum and maintained in a 5% CO_2

418 incubator at 37°C.

419

420 **Cell lysis and immunoblotting assay**

421 Cells were plated 24 h before being treated with inhibitors or starvation medium, and cell
422 confluency did not exceed 70% at the time of harvest. Cell pellets were lysed with either in-house
423 RIPA buffer (50 mM HEPES, 150 mM NaCl, pH 7.6, 1% NP-40, 1% sodium deoxycholate, 0.1%
424 SDS, 10 mM glycerophosphate, 10 mM sodium pyrophosphate, protease inhibitor cocktail,
425 phosphatase inhibitor cocktail) containing 200 μM TCEP, 15 mM $MgCl_2$, and benzonase (Millipore,
426 for RIPA only) or 0.5 % NP40 buffer (50 mM HEPES HCl, 150 mM NaCl, pH 7.4) containing
427 protease inhibitors, phosphatase inhibitors, and 200 μM TCEP. Lysates in RIPA buffer were then
428 sonicated, whereas lysates in NP40 buffer were pipetted and centrifuged at 7,000 rpm for 1 min
429 without sonication. Bradford assay was performed to measure the protein concentration, and the
430 normalized cell lysates were denatured by adding LDS supplemented with 50 mM DTT, followed
431 by boiling at 90 °C for 5 minutes. Less than 30 µg of each lysate was loaded onto the 4-12%
432 NuPAGE Bis-Tris gel (Thermo Fisher Scientific), followed by SDS-PAGE with MES running buffer.
433 Following transfer to PVDF membranes (0.45 µm or 0.2 µm, Millipore), blocking was performed
434 with 5% non-fat milk at room temperature for 15 min, then incubated with primary antibodies
435 overnight at 4°C. After the incubation with primary antibobies, membranes were washed with
436 TBST and further incubated with fluorescent IRDye antibody (1:20000) for 1 h at room
437 temperature. The membrane was then imaged using Chemidoc MP (Biorad).

438

439 **Total proteomics analysis using TMTpro**

440 The total proteomics analyses were performed based on the previously reported method.(22)
441 Briefly, cells are plated into a 10 cm dish per condition, a total of 16 dishes. 24 h later, dTAGv1
442 (100 nM), Hymeglusin (5 µM), or Simvastatin (10 µM) were added to cells and incubated for 24
443 h. Cells were then washed with ice-cold PBS five times and lysed with 800 μl of RIPA buffer (50
444 mM HEPES, 150 mM NaCl, pH 7.6, 1% NP-40, 1% sodium deoxycholate, 0.1% SDS, 10 mM
445 glycerophosphate, 10 mM sodium pyrophosphate, protease inhibitor cocktail, Phosphatase
446 inhibitor cocktail, pH 7.5). The lysate was then collected and sonicated three times, followed by
447 Bradford assay to measure the protein concentration. The total protein concentration was
448 adjusted to become 3 mg/ml throughout the samples using RIPA buffer. 125 μg of each protein
449 extract was taken and reduced by incubation in the presence of 5 mM TCEP at 55 ºC for 10 min.
450 After cooling down to room temperature, the lysates were reacted with chloroacetamide solution
451 (final conc. 20 mM) at room temperature for 15 min, followed by chloroform/methanol

452 precipitation. Protein discs were resuspended in 100 mM EPPS (pH 8.5) containing 0.1%
453 RapiGest and digested at 37 ºC overnight with Trypsin (100:1 protein-to-protease ratio). 16-plex
454 tandem mass tag labeling of each sample was performed by adding 10 µL of the 20 ng/mL stock
455 of TMTpro reagent along with acetonitrile to achieve a final acetonitrile concentration of
456 approximately 30% (v/v). Following incubation at room temperature for 1 h, the reaction was
457 quenched with hydroxylamine to a final concentration of 1% (v/v) for 15 min. The TMTpro-labeled
458 samples were pooled together at a 1:1 ratio. The sample was vacuum centrifuged to near dryness
459 and subjected to C18 solid-phase extraction (SPE) (50 mg, Sep-Pak, Waters). Dried TMTpro-
460 labeled sample was resuspended in 100 µL of 10 mM NH_4HCO_3 pH 8.0 and fractionated using
461 BPRP HPLC. Briefly, samples were offline fractionated over a 90 min run into 96 fractions by high
462 pH reverse-phase HPLC (Agilent LC1260) through an aeris peptide xb-c18 column (Phenomenex;
463 250 mm x 3.6 mm) with mobile phase A containing 5% acetonitrile and 10 mM NH_4HCO_3 in LC-
464 MS grade H_2O, and mobile phase B containing 90% acetonitrile and 10 mM NH4HCO3 in LC-MS
465 grade H_2O (both pH 8.0). The 96 resulting fractions were then pooled in a non-continuous manner
466 into 24 fractions (as outlined in Figure S5 of Paulo et al., 2016)(51) for mass spectrometry
467 analysis. Fractions were vacuum centrifuged to near dryness. Each consolidated fraction was
468 desalted via Stage Tip, dried again via vacuum centrifugation, and reconstituted in 5 %
469 acetonitrile, 1 % formic acid for LC-MS/MS processing.
470
471 Mass spectrometry data were acquired using an Orbitrap Eclipse Tribrid mass spectrometer
472 (Thermo Fisher Scientific, San Jose, CA) connected to an UltiMate 3000 RSLCnano system liquid
473 chromatography (LC) pump (Thermo Fisher Scientific, San Jose, CA). Peptides were separated
474 on a 100 µm inner diameter microcapillary column packed in-house with ~ 30 cm of HALO Peptide
475 ES-C18 resin (2.7 µm, 160 Å, Advanced Materials Technology, Wilmington, DE) with a gradient
476 consisting of 5 %–23 % (0-75 min), 23-40 % (75-110 min) (ACN, 0.1% FA) over a 120 min run at
477 ~500 nL/min. 3/10 of each fraction was loaded onto the column for analysis. Proteome analysis
478 used Multi-Notch MS^3-based TMT quantification, combined with Real Time Search analysis
479 software, and the FAIMS Pro Interface (using previously optimized 3 CV parameters), to reduce
480 ion interference. The scan sequence began with an MS^1 spectrum (Orbitrap analysis; resolution
481 120,000 at 200 Th; mass range 400−1500 m/z; maximum injection time 50 ms; automatic gain
482 control (AGC) target $4x10^5$). For MS2 analysis, precursors were selected based on a cycle time
483 of 1.25 sec/CV method (FAIMS CV=-40/-60/-80). MS^2 analysis consisted of collision-induced
484 dissociation (quadrupole ion trap analysis; Rapid scan rate; AGC $1.0x10^4$; isolation window 0.5
485 Th; normalized collision energy (NCE) 35; maximum injection time 35 ms). Monoisotopic peak

assignment was used, and previously interrogated precursors were excluded using a dynamic window (180 s ±10 ppm). Following the acquisition of each MS^2 spectrum, a synchronous-precursor-selection (SPS) API-MS^3 scan was collected on the top 10 most intense ions b or y-ions matched by the online search algorithm in the associated MS^2 spectrum. MS^3 precursors were fragmented by high energy collision-induced dissociation (HCD) and analyzed using the Orbitrap (NCE 45; AGC $2.5x10^5$; maximum injection time 200 ms, resolution was 50,000 at 200 Th). Closeout was set at two peptides per protein per fraction, so that MS^3s were no longer collected for proteins having two peptide spectrum matches (PSMs) that passed quality filters.

Proteomics Data Analysis

Mass spectra were processed using a Comet-based (2020.01 rev. 4) software pipeline (52, 53). Spectra were first converted to mzXML and monoisotopic peaks were re-assigned using Monocle software (54). MS^2 spectra were matched with peptide sequences with a composite sequence database including the Human Reference Proteome (2020-01 - SwissProt entries only) UniProt database, as well as sequences of common contaminants. This database was concatenated with one composed of all protein sequences in the reversed order. Analysis was performed using a 50 ppm precursor ion tolerance. Static modifications included TMTpro tags on lysine residues and peptide N termini (+304.207 Da) and carbamidomethylation of cysteine residues (+57.021 Da). Oxidation of methionine residues (+15.995 Da) was set as a variable modification. Peptide-spectrum matches (PSMs) were adjusted to a 1% false discovery rate (FDR) (55). PSM filtering was performed using a linear discriminant analysis, (56), while considering the following parameters: Comet log expect, different sequence delta Comet log expect, missed cleavages, peptide length, charge state, precursor mass accuracy, and fraction of ions matched. For protein-level comparisons, PSMs were identified, quantified, and collapsed to a 1% peptide false discovery rate (FDR) and then collapsed further to a final protein-level FDR of 1% (57). To generate the smallest set of proteins required to account for all observed peptides, the principles of parsimony were applied. For TMTpro-based reporter ion quantitation, the summed signal-to-noise (S:N) ratio for each TMT channel was first extracted based on the closest matching centroid to the expected mass of the TMT reporter ion (integration tolerance of 0.003 Da). Isotopic impurities of the different TMTpro reagents provided by the manufacturer specifications, were used to adjust reporter ion intensities. Proteins were quantified by summing reporter ion signal-to-noise measurements across all matching PSMs, resulting in a ‘‘summed signal-to-noise’’ measurement. For total proteome, PSMs with poor quality, or isolation specificity less than 0.75, or with TMT reporter summed signal-to-noise ratio that were less than 160 or had no MS^3 spectra

520 were excluded from quantification. For phospho proteome, PSMs with poor quality, MS^2 spectra
521 with 13 or more TMT reporter ion channels missing, or isolation specificity less than 0.8, or with
522 TMT reporter summed signal-to-noise ratio that were less than 160 were excluded from
523 quantification. The AScore algorithm was used to determine the localization of phosphorylation
524 sites (58). AScore is a probability-based approach for high-throughput protein phosphorylation
525 site localization. Precisely, a threshold of 13 relates to 95% confidence in site localization.
526 Protein quantification values were exported for further analysis in Microsoft Excel and
527 Perseus (59). Each reporter ion channel was summed across all quantified proteins and
528 normalized, assuming equal protein loading was achieved for all samples. The maximum and
529 minimum TMT ratio quantifiable was capped at 100-fold. Organellar protein marker annotations
530 were compiled using the proteins that had scored with confidence ''very high'' or ''high'' from a
531 previously published HeLa dataset (60) and additional entries from manually curated literature.
532 Supplemental data tables list all quantified proteins and the TMTpro reporter ratio
533 associated with control channels used for quantitative analysis.
534
535 **IP-MS analysis using Hymeglusin-biotin probe**
536 HEK293T cells were seeded overnight before incubating with media containing 5 μM hymeglusin
537 or vehicle control (DMSO) for 0.5 hrs. Then 5 μM Hymeglusin-biotin was introduced to the cells
538 and incubated for additional 2 hrs. Cells were washed with ice-cold PBS three times. The cells
539 were then lysed with 200 μl of HEPES-NP40 buffer (50 mM HEPES, 150 mM NaCl, pH 7.5,
540 0.25%NP40). The lysate was centrifuged at 7k for 1 min, and the supernatant was collected. The
541 supernatant was then reduced by 5 mM TCEP (10 min, room temperature) and alkylated by
542 chloroacetamide (20 mM final concentration, 15 min, room temperature).
543 $MeOH/CHCl_3$ precipitation was followed to remove any remaining Hymeglusin-biotin in the cell
544 lysates. The white protein disk was then resuspended in 2% SDS (50 mM HEPES 150 mM NaCl,
545 pH7.2, 2.5 mM TCEP) and sonicated once with a tip sonicator and then diluted in HEPES-NP40
546 buffer (final SDS concentration is < 0.5%). Subsequently, 10 μl of high-capacity streptavidin was
547 added to the cell lysates and incubated for 2 hours at r.t.. Flow-through was stored for the quality
548 control immunoblots, and the beads were washed with RIPA X 2, 2%SDS X 3, RIPA X 2, and
549 PBS X 3. The beads were transferred onto hydrophilic PTFE membrane filter cups and washed
550 twice with water. Completely dried beads were resuspended in 50 μl of hexafluoroisopropanol
551 (HFIP), incubated for 5 min with shaking, and eluted by spinning at 5k rpm. 50 μl of HFIP was
552 added to the beads again, and the eluates were combined and dried in speed vac. 6-plex TMT
553 labeling was performed as described in the proteomics sample preparation section.

554 **In-gel fluorescent analysis with HG-fluorescence probes**

555 Recombinant HMGCS1 protein (1 ug) or cell lysates were incubated with 5 μM Hymeglusin-FITC
556 (HG-FL) or Hymeglusin-TMR (HG-TMR) probe at 37°C for 1 h. The labeling reaction was stopped
557 by adding 4X LDS containing DTT and boiling at 90°C for 5 m. The samples were subjected to
558 SDS-PAGE, and the fluorescent signal in the gel was detected by Chemidoc MP (Biorad).

559

560 **Cell viability assay**

561 Cells viability was evaluated using WST1-based colorimetric assay (Roche). 2 x 10^4 cells in 100
562 μl of culture medium were seeded for each well of 96 well plates. Next day, the cells were treated
563 with culture media containing various amounts of simvastatin and 50 nM of dTAGv1. After 24 h,
564 cells were incubated with WST-1 solution, which was diluted to 1:10 with culture medium in the
565 cell culture incubator. After 4 h, the absorbance of samples was measured using a microplate
566 reader. The wavelength to measure the absorbance of formazan product from viable cells was
567 450 nm, and the reference wavelength was 690 nm.

568

569 **Colony formation assay**

570 To evaluate the ability of single cancer cells to form a colony, cells were plated at a concentration
571 of 1,500 cells/well onto 6 well plates (day 0). At day 5 and day 7, the cells were treated with the
572 corresponding chemicals. On day 12, the cells were stained with a crystal violet working solution,
573 which contains 0.5% crystal violet and 4% paraformaldehyde in PBS. Numbers of colonies were
574 counted for each well (n = 2 or 3) and presented as mean ± s.d.

575

576 **Animal Experiments**

577 Animal experiments were performed in compliance with protocols approved by the Research
578 Animal Resource Center and Institutional Animal Care and Use Committee at Memorial Sloan
579 Kettering Cancer Center. 20 Athymic nude mice (nu/nu athymic mice, Charles River Laboratory)
580 were implanted with HCT116 HMGCS1-FKBP12^{F36V} homozygous knock-in (KI) cells through
581 subcutaneous injection of 2 x 10^6 cells per mouse. The treatment was initiated as the tumor size
582 became 200-250 mm^3. Four groups of mice were administered with two treatment regimens over
583 a two-week interval, including saline control, 5mg/kg Simvastatin three times per week via oral
584 gavage, 5 mg/kg dTAGv1 weekly via intraperitoneally injected (IP), and the combination of both
585 Simvastatin and dTAGv1. PBS is used as a vehicle for both simvastatin and dTAGv1. Tumor
586 growth was monitored and recorded twice a week for 40 days, and five mice were used per
587 condition.

588

589 **Quantification and statistical analysis**

590 P values in the volcano plots of the proteomics data were analyzed by two-sided Welch's t-test
591 which was adjusted for multiple comparisons. Comparisons of the quantified data
592 (immunoblotting, colony formation, tumor spheroids) were performed by unpaired Student's t-test;
593 Statistical significance was judged based on p-values; *$p < 0.05$; **$p < 0.01$; ***$p < 0.001$.

594 **DATA AND CODE AVAILABILITY**

595 - All unique identifiers, and web links for publicly available datasets are presented within the
596 main text or the supplementary materials. The proteomic data generated in this paper will
597 be deposited to the MassIVE repository with the dataset identifier: MSV000098111
598 - This paper does not report any original code.
599 - Any additional information required to reanalyze the data reported in this paper is available
600 from the lead contact upon request.

601 **CONFLICT OF INTEREST**

602 The authors declare no competing interests.

603 **ACKNOWLEDGMENTS**

604 We thank Brittany Pham for helping with the cell viability assay. We thank Beth Moorefield, Ph.
605 D., for providing critical feedback and review of the manuscript. We thank Mr. William H. Goodwin
606 and Mrs. Alice Goodwin and the Commonwealth Foundation, and the Center for Experimental
607 Therapeutics at Memorial Sloan Kettering Cancer Center for their support.

608 **AUTHOR CONTRIBUTIONS**

609 Conceptualization, S.A.Y., L.S. and H.A.; methodology, S.A.Y., L.S., Y.R., and A.O.; Investigation,
610 S.A.Y., L.S., Y.R., and A.O.; writing—original draft, S.A.Y., L.S., and H.A.; writing—review &
611 editing, Y.R., A.O. and J.L.; funding acquisition, A.O., J.L., and H.A.; supervision, H.A.

612 **FUNDING AND ADDITIONAL INFORMATION**

613 This work was supported by the MSKCC Josie Robertson Foundation (H.A.), NIH R35 CA232130
614 (J.S. L), and partly by the Memorial Sloan Kettering Cancer Center Support Grant P30CA008748
615 (A.O., J.S.L., and H.A.)

Figure 1

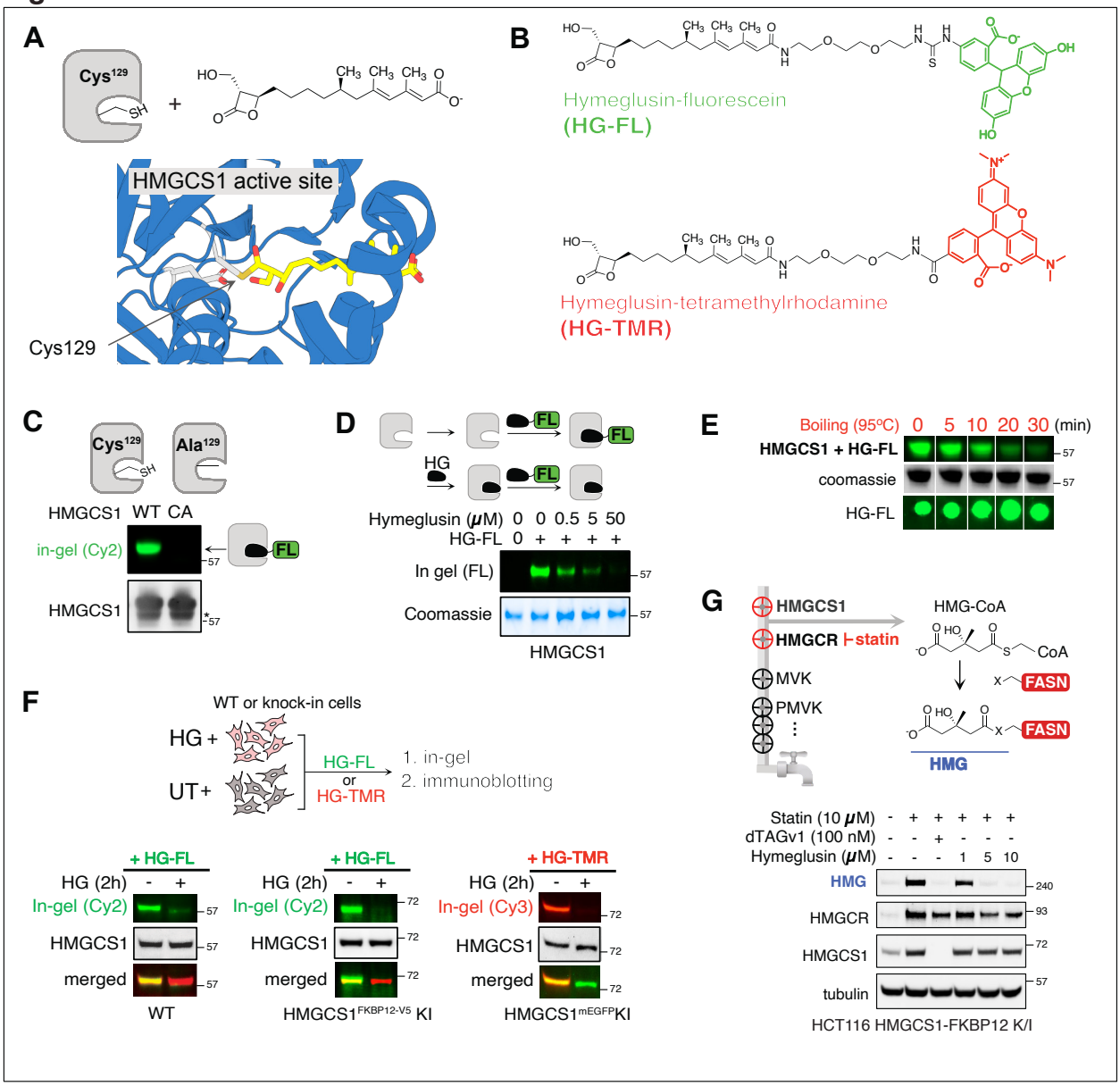
A
Cys129
SH
HMGCS1 active site
Cys129
B
Hymeglusin-fluorescein
(HG-FL)
Hymeglusin-tetramethylrhodamine
(HG-TMR)
C
Cys129
Ala129
HMGCS1 WT CA
in-gel (Cy2)
FL
HMGCS1
57
D
HG
FL
Hymeglusin (μM) 0 0 0.5 5 50
HG-FL 0 + + + +
In gel (FL)
Coomassie
HMGCS1
E
Boiling (95ºC) 0 5 10 20 30 (min)
HMGCS1 + HG-FL
coomassie
HG-FL
G
HMGCS1
HMGCR
statin
MVK
PMVK
HMG-CoA
CoA
FASN
HMG
Statin (10 μM) - + + + + +
dTAGv1 (100 nM) - - + - - -
Hymeglusin (μM) - - - 1 5 10
HMG
HMGCR
HMGCS1
tubulin
240
93
72
57
HCT116 HMGCS1-FKBP12 K/I
F
WT or knock-in cells
HG +
UT+
HG-FL
or
HG-TMR
1. in-gel
2. immunoblotting
+ HG-FL
HG (2h) - +
In-gel (Cy2)
HMGCS1
merged
WT
HMGCS1FKBP12-V5 KI
+ HG-TMR
In-gel (Cy3)
HMGCS1mEGFPKI

627 **FIGURE 1. Hymeglusin-fluorescence conjugates serve as activity-based probes for HMGCS1.**
628 (A) A schematic of the HMGCS1 and Hymeglusin (top) and the zoomed-in co-crystal structure of the
629 Hymeglusin-bound HMGCS1 (bottom, PDB: 2F9A)
630 (B) Chemical structures of the Hymeglusin-fluorescein (HG-FL) and Hymeglusin-tetramethylrhodamine
631 probes (HG-TMR).
632 (C) Comparative in-gel fluorescence assay of wild-type (WT) or a catalytically inactive HMGCS1 mutant
633 (C129A, CA) confirms the labeling of the catalytic cysteine of HMGCS1 with HG-FL.
634 (D) Top: scheme of the HG-FL competition reaction *in vitro*. Bottom: incubating recombinant HMGCS1 (1
635 µg) with increasing concentrations of Hymeglusin for 30 minutes results in a decrease of HG-FL labeled
636 HMGCS1.
637 (E) The labeling of HMGCS1 by HG-FL was reversed after boiling at 95°C for at least 20 minutes in a buffer
638 containing 2% LDS and 50 mM DTT. SDS-PAGE resolved HMGCS1 before the in-gel fluorescence
639 analysis, while the stability of the HG-FL probe in the given conditions was assessed by dot blot in parallel.
640 (F) HEK293T WT and HCT116 knock-in (KI) (HMGCS1-FKBP12^{F36V} or HMGCS1-mEGFP) cells were
641 treated with Hymeglusin (4 μM for WT, 0.5 μM for KI, 2 hours) or left untreated, followed by cell lysis and
642 incubation with HG-FL or HG-TMR for one hour. After in-gel fluorescence analysis, the gels were
643 transferred to the PVDF membrane for immunoblotting using an anti-HMGCS1 antibody.
644 (G) HMGCR inhibition by statins leads to the accumulation of HMG-CoA in cells. This results in the non-
645 enzymatic modification of several residues in the FASN active site by the HMG moiety, which can be
646 detected by the anti-HMG antibody (top). HCT116 cells expressing endogenous HMGCS1-FKBP12^{F36V}
647 were treated with the indicated chemicals for 24 hours, followed by immunoblotting analysis using anti-
648 HMG, anti-HMGCR, anti-HMGCS1, and anti-tubulin antibodies (bottom).
649
650
651
652
653

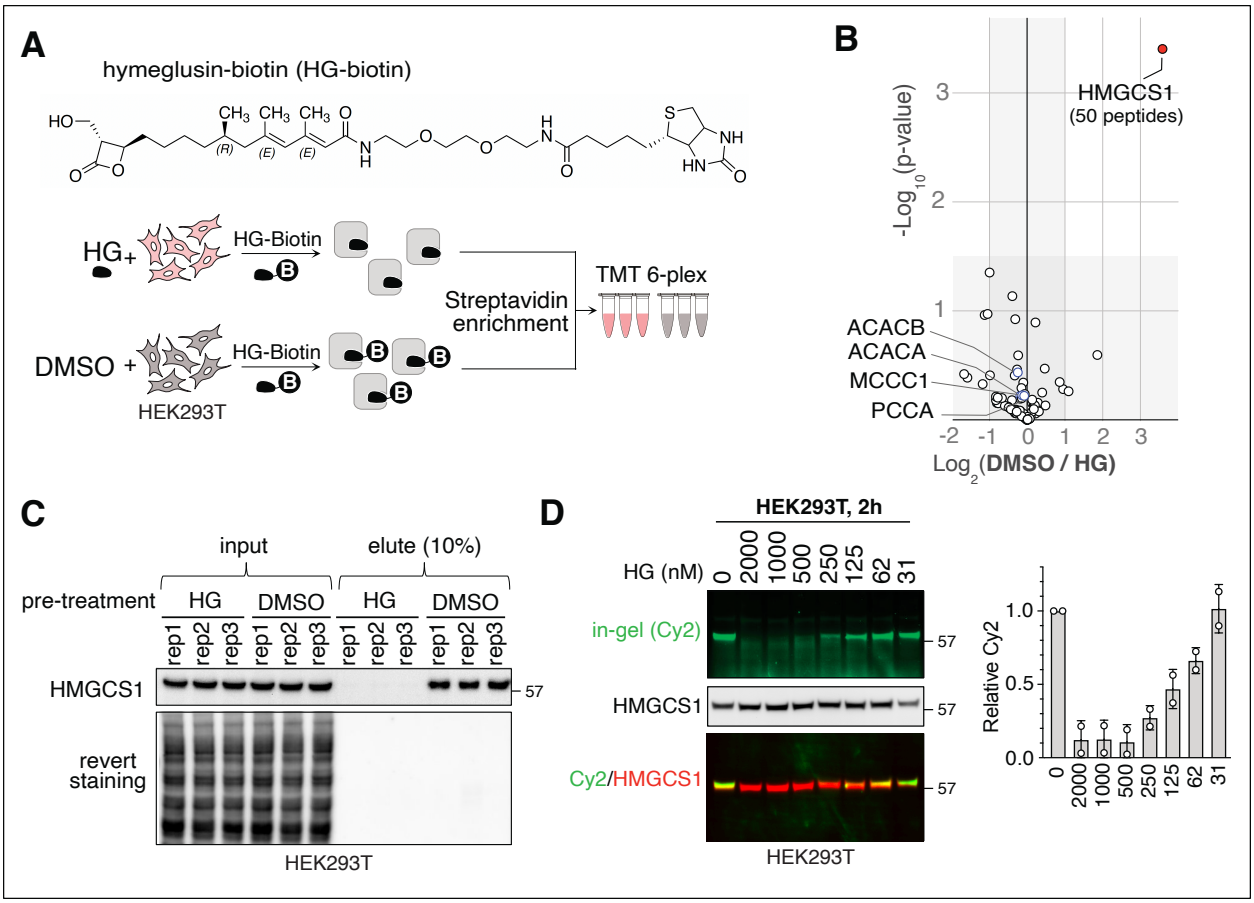

FIGURE 2. Hymeglusin is a highly selective inhibitor of HMGCS1 in human cells.

(A) The structure of the Hymeglusin-biotin probe is shown at the top, and the workflow of competitive affinity purification mass-spectrometry (AP-MS) using Hymeglusin-biotin combined with TMT-6 plex methods is shown at the bottom.

(B) HEK293T cells were either treated with HG (1 μM, 30 min) or DMSO, followed by further incubation with the in-house HG-biotin probe (1 μM, 2 h). After streptavidin beads enrichment, the eluates were analyzed through tandem-mass-tag-based proteomic analysis. The proteomic data is presented as a volcano plot of the $-\log_{10}$-transformed p-value versus the $\log_2$-transformed ratio of DMSO/Hymeglusin pre-treated cells. n = 3 biological replicates. p-values were calculated by two-sided Welch's t-test (adjusted to 1% FDR for multiple comparisons).

(C) HEK293T cells were treated as described in panel A. After streptavidin enrichment, the eluates were subjected to immunoblotting using the anti-HMGCS1 antibody. Rep: replicate.

(D) HEK293T cells were treated with increasing concentrations of Hymeglusin for 2 hours, followed by HG-FL treatment and in-gel fluorescence analysis. The same extracts were then transferred to a PVDF membrane to probe for HMGCS1 using immunoblotting. The average of two replicates is shown on the right.

Figure 3

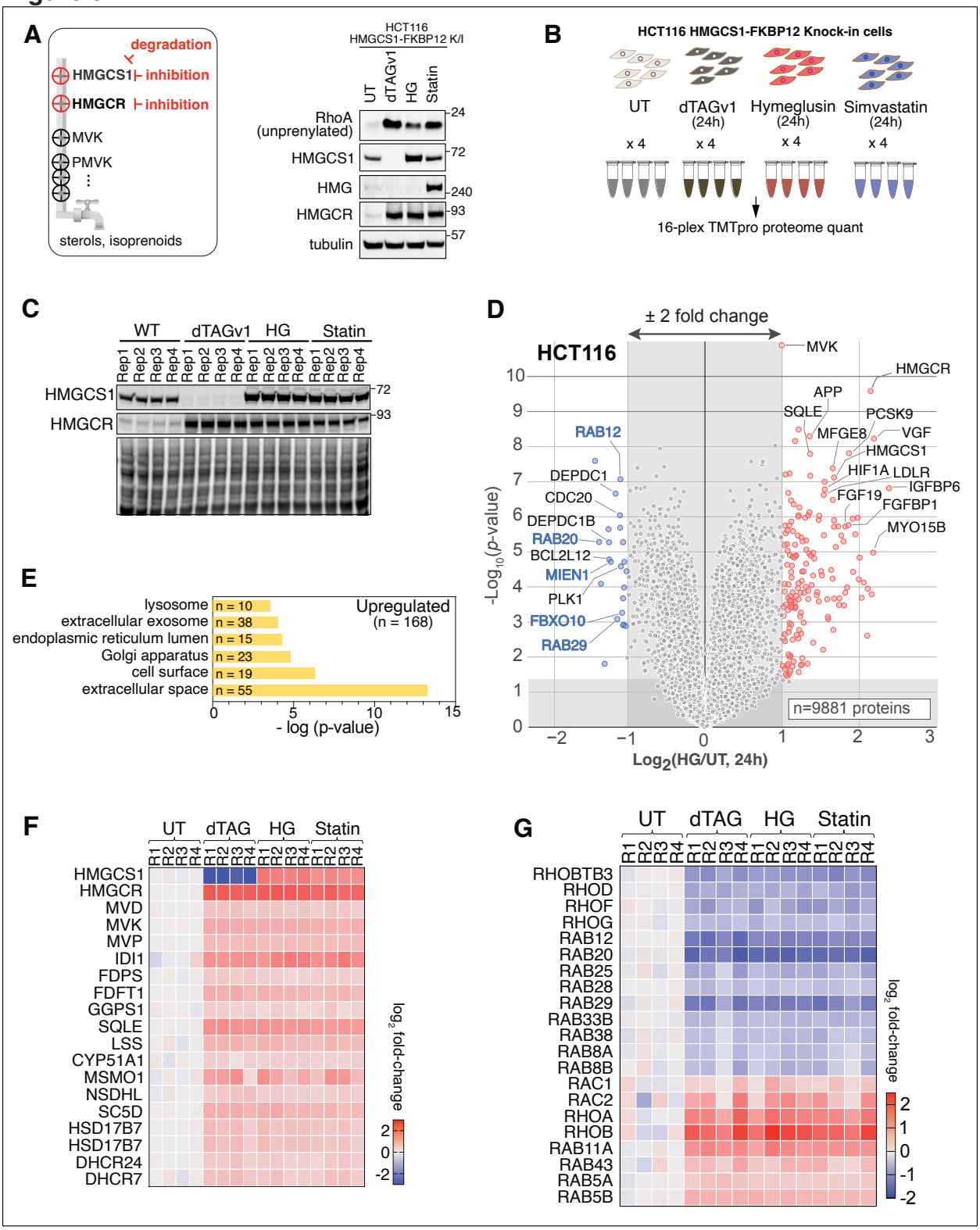
A
degradation
HMGCS1
inhibition
HMGCR
inhibition
MVK
PMVK
sterols, isoprenoids
HCT116
HMGCS1-FKBP12 K/I
UT
dTAGv1
HG
Statin
RhoA (unprenylated)
HMGCS1
HMG
HMGCR
tubulin
24
72
240
93
57
B
HCT116 HMGCS1-FKBP12 Knock-in cells
UT
dTAGv1 (24h)
Hymeglusin (24h)
Simvastatin (24h)
x 4
16-plex TMTpro proteome quant
C
WT
dTAGv1
HG
Statin
Rep1
Rep2
Rep3
Rep4
HMGCS1
HMGCR
72
93
D
± 2 fold change
HCT116
MVK
HMGCR
APP
SQLE
PCSK9
MFGE8
VGF
HMGCS1
HIF1A
LDLR
IGFBP6
FGF19
FGFBP1
MYO15B
RAB12
DEPDC1
CDC20
DEPDC1B
RAB20
BCL2L12
MIEN1
PLK1
FBXO10
RAB29
n=9881 proteins
-Log10(p-value)
Log2(HG/UT, 24h)
E
Upregulated (n = 168)
lysosome
extracellular exosome
endoplasmic reticulum lumen
Golgi apparatus
cell surface
extracellular space
n = 10
n = 38
n = 15
n = 23
n = 19
n = 55
- log (p-value)
F
UT
dTAG
HG
Statin
R1
R2
R3
R4
HMGCS1
HMGCR
MVD
MVK
MVP
IDI1
FDPS
FDFT1
GGPS1
SQLE
LSS
CYP51A1
MSMO1
NSDHL
SC5D
HSD17B7
HSD17B7
DHCR24
DHCR7
log2 fold-change
G
RHOBTB3
RHOD
RHOF
RHOG
RAB12
RAB20
RAB25
RAB28
RAB29
RAB33B
RAB38
RAB8A
RAB8B
RAC1
RAC2
RHOA
RHOB
RAB11A
RAB43
RAB5A
RAB5B
log2 fold-change

675 **FIGURE 3. Perturbing HMGCS1 by Hymeglusin and HMGCR by Simvastatin leads to identical global**
676 **proteome changes.**
677 (A) left panel: A schematic illustrating the mevalonate pathway flux. Three perturbation approaches—
678 inhibition or degradation of HMGCS1 and inhibition of HMGCR—are compared for their effects on global
679 proteome changes. Right panel: HCT116 HMGCS1-FKBP12^{F36V} knock-in cells were treated with dTAGv1
680 (100 nM, for HMGCS1 degradation), Hymeglusin (5 μM, for HMGCS1 inhibition), and Simvastatin (10 μM,
681 for HMGCR inhibition) for 48 hours. The cell extracts were then probed with the indicated antibodies to
682 check the cellular response.
683 (B) The 16-plex TMTpro approach was utilized to compare the global proteome changes after 24 hours of
684 the specified small molecule treatment.
685 (C) HEK293T cells treated as described in panel B were probed with the indicated antibodies as a quality
686 control step prior to proteomic analysis.
687 (D) Analysis of the TMT-plex data is presented as a volcano plot of the —$\log_{10}$-transformed p-value versus
688 the $\log_2$-transformed ratio of Hymeglusin treated/untreated (UT) conditions for HCT116 HMGCS1-
689 FKBP12^{F36V} knock-in cells. p values were calculated by two-sided Welch's t-test (adjusted to 1% FDR for
690 multiple comparisons). A total of 9881 proteins were quantified. n = 4 biological replicates.
691 (E) Gene ontology analyses of the statistically significant upregulated proteins (168 proteins) with more
692 than 2-fold changes are shown. N represents the number of proteins counted in the category.
693 (F) 19 quantified proteins in the mevalonate/sterol pathway were curated and their log2 fold-changes are
694 presented as a heat map. dTAG treatment led to the steep depletion of HMGCS1.
695 (G) Representative families of isoprenylation targets (Rho, Rab, Rheb, and Ras proteins) were curated from
696 1,200 statistically significant hits and plotted as a heatmap. No Ras or Rheb proteins showed statistically
697 significant change upon treatment.
698

Figure 4.

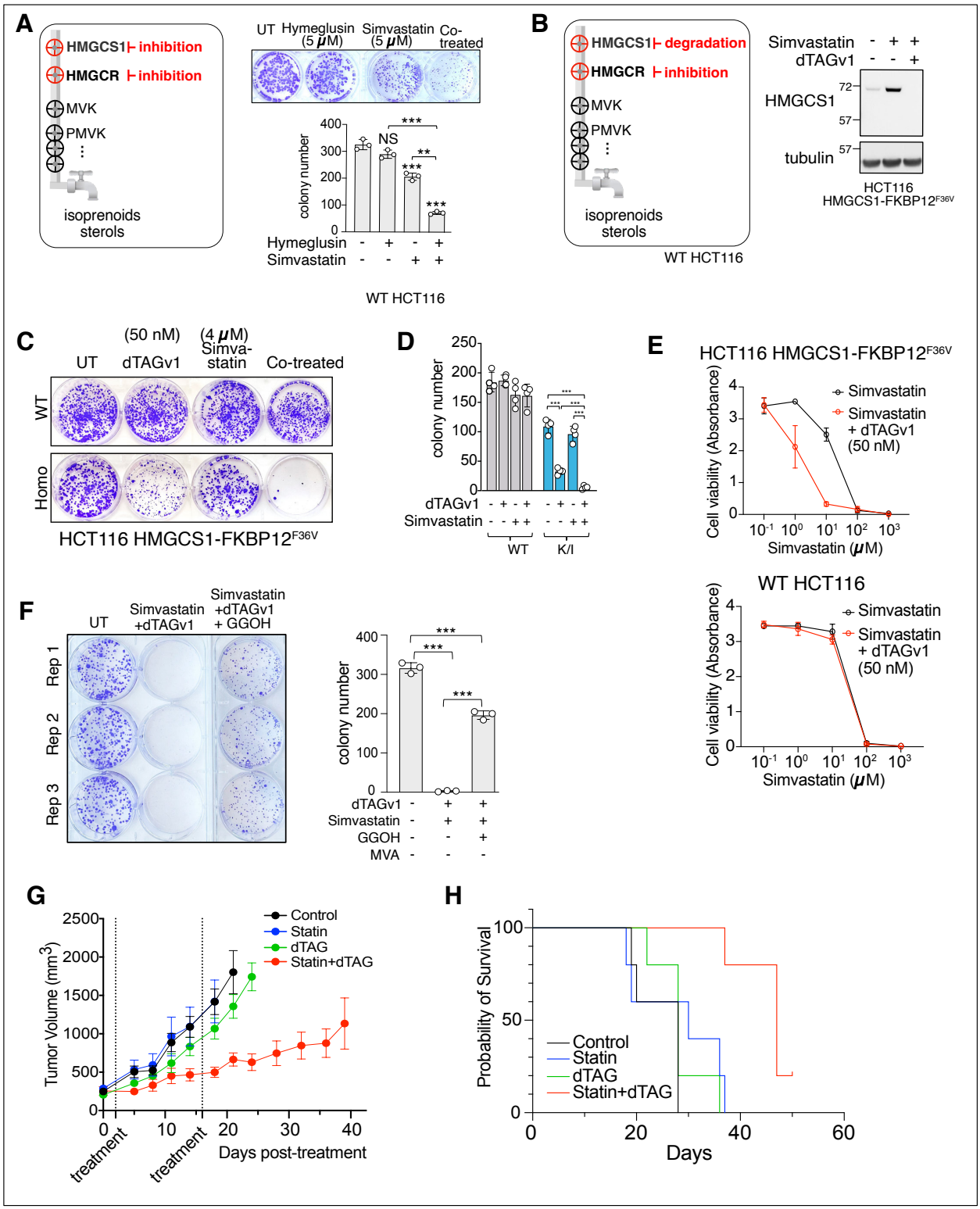
A
HMGCS1 inhibition
HMGCR inhibition
MVK
PMVK
isoprenoids
sterols
UT
Hymeglusin (5 μM)
Simvastatin (5 μM)
Co-treated
colony number
NS
Hymeglusin
Simvastatin
WT HCT116
B
HMGCS1 degradation
HMGCR inhibition
MVK
PMVK
isoprenoids
sterols
WT HCT116
Simvastatin
dTAGv1
HMGCS1
tubulin
HCT116
HMGCS1-FKBP12F36V
C
UT
(50 nM) dTAGv1
(4 μM) Simva-statin
Co-treated
WT
Homo
HCT116 HMGCS1-FKBP12F36V
D
colony number
dTAGv1
Simvastatin
WT
K/I
E
HCT116 HMGCS1-FKBP12F36V
Cell viability (Absorbance)
Simvastatin
Simvastatin + dTAGv1 (50 nM)
Simvastatin (μM)
WT HCT116
F
UT
Simvastatin +dTAGv1
Simvastatin +dTAGv1 + GGOH
Rep 1
Rep 2
Rep 3
colony number
dTAGv1
Simvastatin
GGOH
MVA
G
Tumor Volume (mm3)
Control
Statin
dTAG
Statin+dTAG
treatment
treatment
Days post-treatment
H
Probability of Survival
Control
Statin
dTAG
Statin+dTAG
Days

703 **FIGURE 4. Combinatory targeting HMGCS1 and HMGCR exhibit synergistic anti-tumor effects.**
704 (A) The left panel presents a schematic illustration of the combinatorial inhibition of HMGCS1 and HMGCR.
705 In the right panel, the colony formation assay results for HMGCS1-FKBP12^{F36V} K/I HCT116 cells are shown,
706 where treatments involved either Hymeglusin (5 μM), Simvastatin (5 μM), or a combination of both
707 inhibitors. Corresponding inhibitors were applied on days 5 and 7 after seeding, and the colony numbers
708 were counted on day 12. The accompanying quantification graph displays the means ± SD from biological
709 triplicates.
710 (B) The left panel illustrates the degradation of HMGCS1 and the inhibition of HMGCR as a combinatorial
711 approach to target the mevalonate pathway. The right panel shows the induction of HMGCS1 following
712 Simvastatin treatment, which was completely reversed by dTAGv1 treatment due to the induced
713 degradation in HCT116 cells expressing endogenous HMGCS1-FKBP12^{F36V}.
714 (C) HMGCS1 degradation by dTAGv1 (50 nM) increases the inhibitory effects of Simvastatin (4 μM) on the
715 colony-forming activity of HCT116 HMGCS1-FKBP12^{F36V} cells.
716 (D) Means ± s.d. of biological quadruplicate data from Panel C.
717 (E) HMGCS1 degradation by the dTAG system reduces the IC_{50} value of Simvastatin by 10-fold in HCT116
718 HMGCS1-FKBP12^{F36V} knock-in cells (top). Cell viability was assessed 24 hours after treating the
719 corresponding cells with increasing concentrations of Simvastatin and dTAGv1 (50 nM). The wild-type
720 HCT116 did not show the synergistic effect of dTAGv1 and Simvastatin (bottom).
721 (F) The anti-colony formation effect induced by the HMGCS1 degradation and HMGCR inhibition was
722 rescued by supplementation of geranylgeraniol (GGOH, 40 μM). HCT116 HMGCS1-FKBP12^{F36V} K/I cells
723 were treated with dTAGv1 (50 nM) and Simvastatin (4 μM) on days 5 and 7, post-seeding. GGOH (40 μM)
724 was added to the media of the corresponding cells on days 5 and 7. Means ± s.d. of biological triplicate
725 data is shown on the right.
726 (G) HMGCS1-FKBP12^{F36V} K/I HCT116 cells were implanted into nude mice. When the tumor size reached
727 200 – 250 mm^3, we administrated two treatment regimens (shown in dotted vertical lines), including saline
728 control, 5 mg/kg Simvastatin via gavage three times a week, weekly 5mg/kg dTAGv1 through i.p., and the
729 combination of both dTAGv1 and Simvastatin. Degradation of HMGCS1 by the dTAG system potentiates
730 the tumor growth-suppressing effect of Simvastatin. n = 5 mice for each condition.
731 (H) Survival probability analysis of the mice presented in Panel H using Kaplan-Meier software reveals
732 extended mortality in the dTAG and Statin co-treatment groups compared to the other control groups.
733
734
735
736
737
738

Figure 5

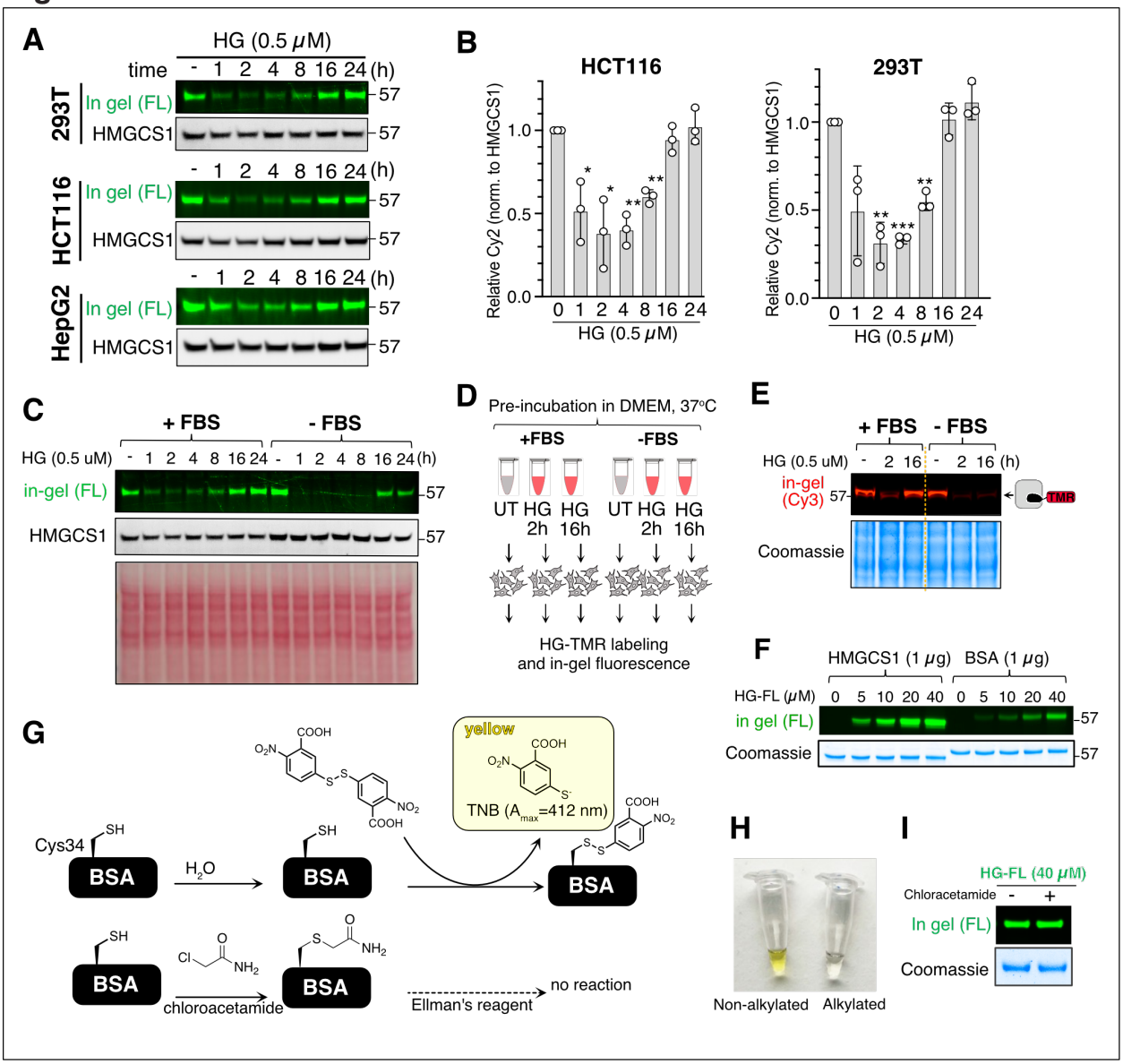
A
HG (0.5 μM)
time - 1 2 4 8 16 24 (h)
293T
In gel (FL)
HMGCS1
HCT116
HepG2
57
B
HCT116
293T
Relative Cy2 (norm. to HMGCS1)
HG (0.5 μM)
C
+ FBS
- FBS
HG (0.5 uM)
in-gel (FL)
D
Pre-incubation in DMEM, 37°C
+FBS
-FBS
UT HG 2h HG 16h
HG-TMR labeling and in-gel fluorescence
E
HG (0.5 uM)
in-gel (Cy3)
TMR
Coomassie
F
HMGCS1 (1 μg)
BSA (1 μg)
HG-FL (μM)
in gel (FL)
Coomassie
G
Cys34
BSA
H2O
yellow
TNB (Amax=412 nm)
chloroacetamide
Ellman's reagent
no reaction
H
Non-alkylated
Alkylated
I
HG-FL (40 μM)
Chloracetamide
In gel (FL)
Coomassie

751 **FIGURE 5. Hymeglusin exhibits poor serum stability.**
752 (A) HCT116, HEK293T, and HepG2 cells were treated with Hymeglusin (0.5 μM) for the indicated time
753 points, followed by lysis and reaction with the HG-FL probe. In-gel fluorescence analysis and
754 immunoblotting were then performed
755 (B) The quantification of relative fluorescence intensity from three replicate experiments in panel A is
756 presented. Mean ± s.d.
757 (C) The absence of FBS in the cell culture media delays the appearance of active HMGCS1 with free
758 catalytic cysteine after prolonged treatment of cells with Hymeglusin.
759 (D) A workflow to test the effect of fetal bovine serum (FBS) on the stability of Hymeglusin. 0.5 μM of
760 Hymeglusin was added to DMEM supplemented with or without 10% FBS. The media was then incubated
761 at 37°C for 2 or 16 hours before being added to HEK293T cells.
762 (E) HEK293T cells treated as in panel D were subjected to in-gel fluorescence analysis.
763 (F) *In vitro* incubation of HG-FL with recombinant HMGCS1 (1 μg) or BSA (1 μg) for 1 hour produces a
764 green fluorescence signal in the relevant molecular weight regions, indicating a strong interaction between
765 HG-FL and BSA.
766 (G) Scheme of Ellman's reagent, which turns the solution into a yellow visible color when reacted with thiol
767 by producing TNB.
768 (H) A portion of the samples treated as in G were reacted with Ellman's reagent. Specifically, BSA was
769 incubated with water or chloroacetamide for 10 minutes, followed by the addition of Ellman's reagent. The
770 water pre-treated sample turned into the expected yellow solution, while the chloroacetamide pre-treated
771 BSA solution did not change color, indicating the loss of free thiol due to alkylation.
772 (I) The remaining portion of the samples in panels G and H was then incubated with HG-FL, which showed
773 an equal level of green fluorescence signal.
774
775
776
777
778
779
780
781
782
783
784
785
786
787

Figure S1

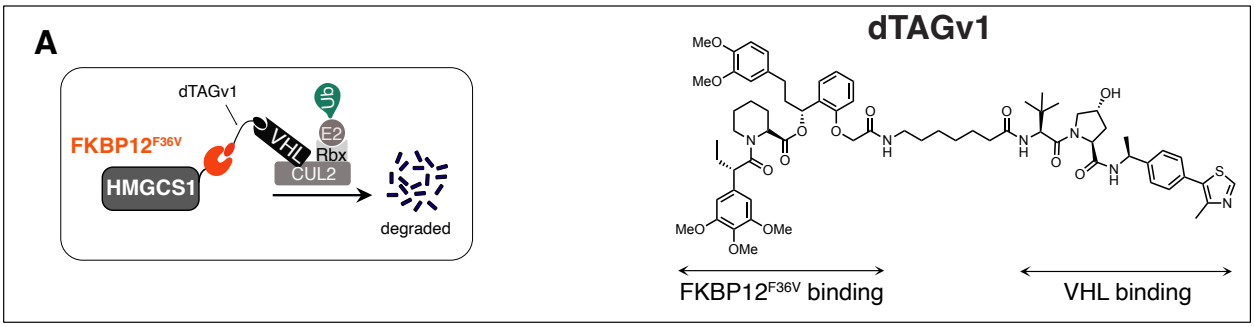

SI FIGURE 1. Overview of induced proteolysis by the dTAG system (Related to Figure 1).
(A) The schematic of the dTAG system (left) and chemical structure of the dTAGv1 ligand (right). This bifunctional ligand can bring VHL closer to the FKBP12^{F36V} mutant.

Figure S2

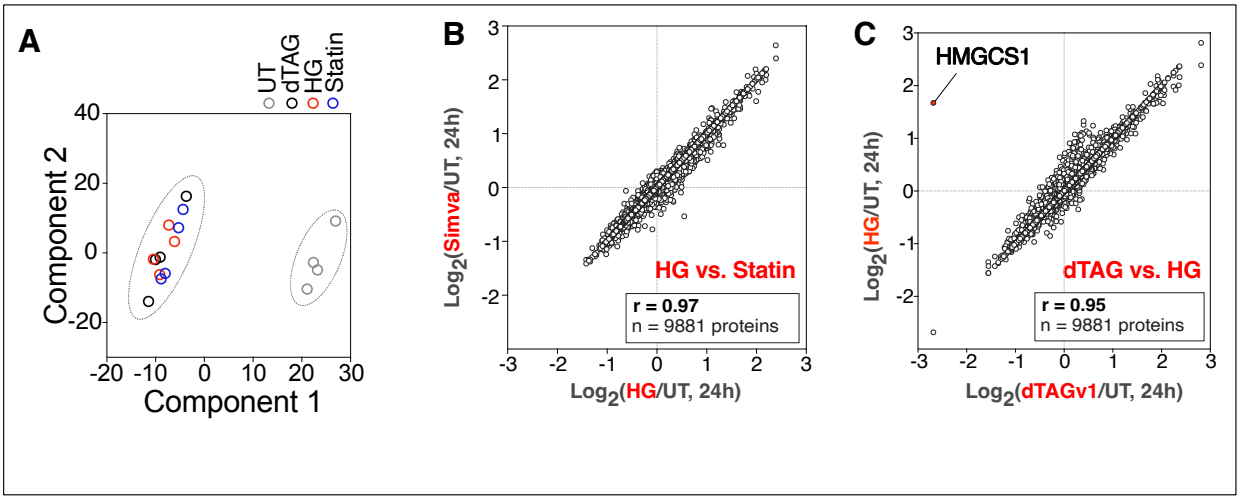

SI FIGURE 2. Global proteomic changes induced upon MVP inhibition (Related to Figure 3).
(A) Principal component analysis (PCA) of the total proteomics dataset, prepared as shown in Fig. 3B, indicates that dTAG, HG, and Statin-treated cells are grouped together.
(B,C) 9881 proteins were plotted for the $\log_2$-ratio of (Simvastatin/DMSO) against the $\log_2$-ratio of (HG/DMSO) for panel B, and $\log_2$-ratio of (Hymeglusin/DMSO) against the $\log_2$-ratio of (dTAGv1/DMSO) for panel C. N = 4 replicates. p values were calculated by two-sided Welch's t-test (adjusted to 1% FDR for multiple comparisons). A total of 9881 proteins were quantified. n = 4 biological replicates.

Figure S3

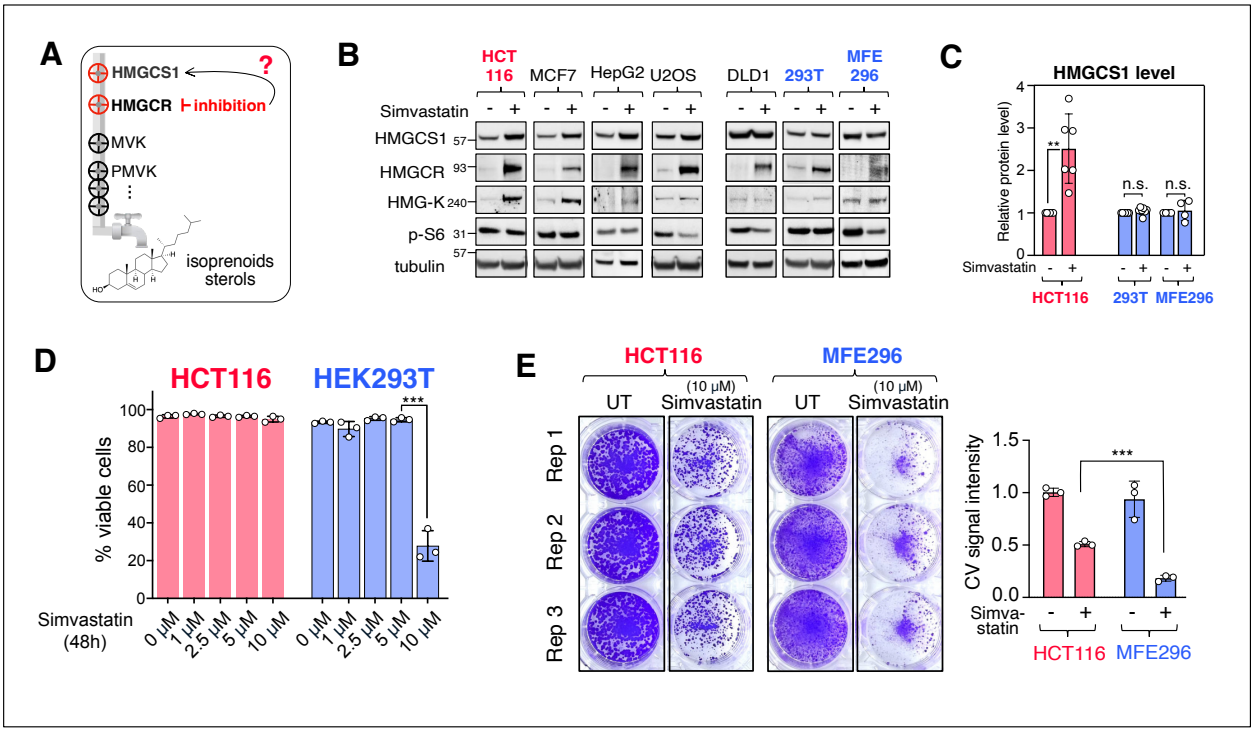

SI FIGURE 3. Relation between HMGCS1 upregulation and statin resistance (Related to Figure 4).

(A) A schematic showing the relationship between HMGCR inhibition and HMGCS1 up-regulation.

(B) The level of HMGCS1 upon Simvastatin treatment for 24 hours was assessed in seven different cell lines using immunoblotting analysis. Indicated cells were treated with Simvastatin (10 μM, 24h), followed by immunoblotting with indicated antibodies.

(C) The relative level of HMGCS1 protein was quantified from the experimental replicates shown in panel B, with n > 4 replicates. Mean ± s.d.

(D) Flow cytometry analysis of DAPI-stained versus unstained cells was conducted to evaluate cell viability after treating indicated cells with increasing concentrations of Simvastatin for 48 hours.

(E) Coloniformation assay with or without Simvastatin treatment was performed on MFE296 and HCT116 cell lines. The total signal intensity per plate, relative to the untreated condition, is presented on the right. Mean ± s.d. n = 3 replicates.

Figure S4

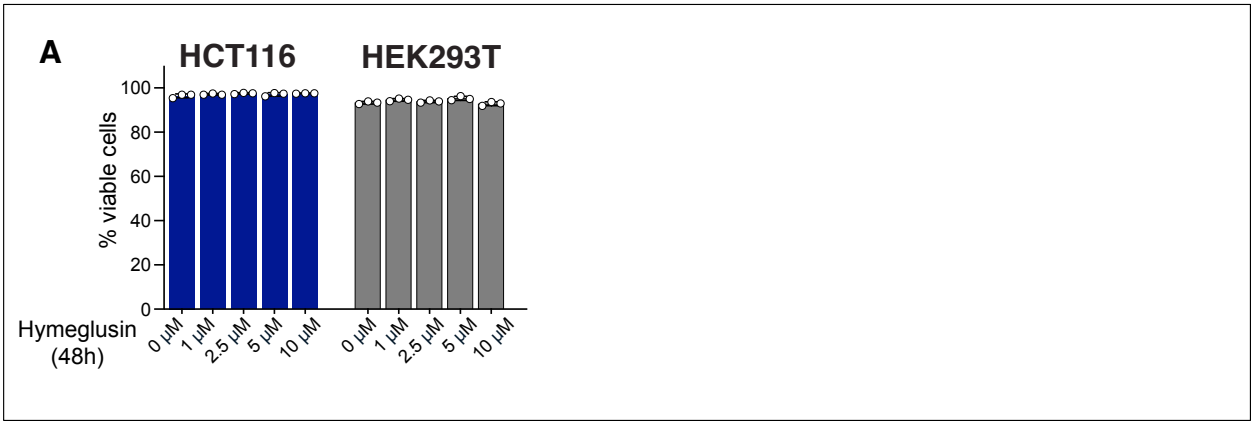

SI FIGURE 4. Limited efficacy of Hymeglusin on cell proliferation (Related to Figure 6). (A) HEK293T and HCT116 cells were treated with increasing concentration of Hymeglusin, followed by cell viability assay using flow-cytometry method.

TABLE S1. AFFINITY-PROTEOMICS USING HYMEGLUSIN-BIOTIN PROBE (RELATED TO FIGURE 2). HEK293T cells, pretreated with Hymeglusin or DMSO, were further treated with Hymeglusin-biotin, followed by streptavidin enrichment and TMT-6plex analysis.

TABLE S2. COMPARATIVE PROTEOMICS UPON MVP INHIBITION (RELATED TO FIGURE 3). TMT-based proteomic data for HCT116 HMGCS1-FKBP12^{F36V} cells following treatment with DMSO, dTAGv1, Hymeglusin, and Simvastatin for 24 hours.

TABLE S3. KEY RESOURCES TABLE. Resources of materials used in this study.

847 **REFERENCES**

848 1. Brown, M. S., and Goldstein, J. L. (1986) A receptor-mediated pathway for cholesterol homeostasis
849 *Science* **232**, 34-47

850 2. Goldstein, J. L., and Brown, M. S. (1990) Regulation of the mevalonate pathway *Nature* **343**, 425-
851 430

852 3. Luo, J., Yang, H., and Song, B. L. (2020) Mechanisms and regulation of cholesterol homeostasis
853 *Nat Rev Mol Cell Biol* **21**, 225-245

854 4. Mullen, P. J., Yu, R., Longo, J., Archer, M. C., and Penn, L. Z. (2016) The interplay between cell
855 signalling and the mevalonate pathway in cancer *Nat Rev Cancer* **16**, 718-731

856 5. Juarez, D., and Fruman, D. A. (2021) Targeting the Mevalonate Pathway in Cancer *Trends Cancer*
857 **7**, 525-540

858 6. Clendening, J. W., Pandyra, A., Boutros, P. C., El Ghamrasni, S., Khosravi, F., Trentin, G. A. *et al.*
859 (2010) Dysregulation of the mevalonate pathway promotes transformation *Proc Natl Acad Sci U S*
860 *A* **107**, 15051-15056

861 7. Jiang, P., Mukthavaram, R., Chao, Y., Nomura, N., Bharati, I. S., Fogal, V. *et al.* (2014) In vitro and
862 in vivo anticancer effects of mevalonate pathway modulation on human cancer cells *Br J Cancer*
863 **111**, 1562-1571

864 8. Kuzu, O. F., Noory, M. A., and Robertson, G. P. (2016) The Role of Cholesterol in Cancer *Cancer*
865 *Res* **76**, 2063-2070

866 9. Karlic, H., Thaler, R., Gerner, C., Grunt, T., Proestling, K., Haider, F. *et al.* (2015) Inhibition of the
867 mevalonate pathway affects epigenetic regulation in cancer cells *Cancer Genet* **208**, 241-252

868 10. Zhou, C., Li, J., Sun, X., Zhao, L., Zhan, H., Liang, H. *et al.* (2024) Targeting HMGCS1 restores
869 chemotherapy sensitivity in acute myeloid leukemia *Blood Sci* **6**, e00192

870 11. Pandyra, A. A., Mullen, P. J., Goard, C. A., Ericson, E., Sharma, P., Kalkat, M. *et al.* (2015)
871 Genome-wide RNAi analysis reveals that simultaneous inhibition of specific mevalonate pathway
872 genes potentiates tumor cell death *Oncotarget* **6**, 26909-26921

873 12. Malhi, M., Norris, M. J., Duan, W., Moraes, T. J., and Maynes, J. T. (2021) Statin-mediated
874 disruption of Rho GTPase prenylation and activity inhibits respiratory syncytial virus infection
875 *Commun Biol* **4**, 1239

876 13. Jiao, Z., Cai, H., Long, Y., Sirka, O. K., Padmanaban, V., Ewald, A. J. *et al.* (2020) Statin-induced
877 GGPP depletion blocks macropinocytosis and starves cells with oncogenic defects *Proc Natl Acad*
878 *Sci U S A* **117**, 4158-4168

879 14. Whyte, D. B., Kirschmeier, P., Hockenberry, T. N., Nunez-Oliva, I., James, L., Catino, J. J. *et al.*
880 (1997) K- and N-Ras are geranylgeranylated in cells treated with farnesyl protein transferase
881 inhibitors *J Biol Chem* **272**, 14459-14464

882 15. Kohl, N. E., Mosser, S. D., deSolms, S. J., Giuliani, E. A., Pompliano, D. L., Graham, S. L. *et al.*
883 (1993) Selective inhibition of ras-dependent transformation by a farnesyltransferase inhibitor
884 *Science* **260**, 1934-1937

885 16. Philips, M. R., and Cox, A. D. (2007) Geranylgeranyltransferase I as a target for anti-cancer drugs
886 *J Clin Invest* **117**, 1223-1225

887 17. Ullah, N., Mansha, M., and Casey, P. J. (2016) Protein Geranylgeranyltransferase Type 1 as a
888 Target in Cancer *Curr Cancer Drug Targets* **16**, 563-571

889 18. Drake, M. T., Clarke, B. L., and Khosla, S. (2008) Bisphosphonates: mechanism of action and role
890 in clinical practice *Mayo Clin Proc* **83**, 1032-1045

891 19. Lin, J. H. (1996) Bisphosphonates: a review of their pharmacokinetic properties *Bone* **18**, 75-85

892 20. Jiang, W., Hu, J. W., He, X. R., Jin, W. L., and He, X. Y. (2021) Statins: a repurposed drug to fight
893 cancer *J Exp Clin Cancer Res* **40**, 241

894 21. Longo, J., van Leeuwen, J. E., Elbaz, M., Branchard, E., and Penn, L. Z. (2020) Statins as
895 Anticancer Agents in the Era of Precision Medicine *Clin Cancer Res* **26**, 5791-5800

896 22. Yi, S. A., Sepic, S., Schulman, B. A., Ordureau, A., and An, H. (2024) mTORC1-CTLH E3 ligase
897 regulates the degradation of HMG-CoA synthase 1 through the Pro/N-degron pathway *Mol Cell* **84**,
898 2166-2184 e2169

899 23. Zhou, C., Wang, Z., Yang, S., Li, H., and Zhao, L. (2022) Hymeglusin Enhances the Pro-Apoptotic
900 Effects of Venetoclax in Acute Myeloid Leukemia *Front Oncol* **12**, 864430

901 24. Casselbrant, A., Elias, E., Hallersund, P., Elebring, E., Cervin, J., Fandriks, L. *et al.* (2024) Intestinal
902 Ketogenesis and Permeability *Int J Mol Sci* **25**,

903 25. Greenspan, M. D., Yudkovitz, J. B., Lo, C. Y., Chen, J. S., Alberts, A. W., Hunt, V. M. *et al.* (1987)
904 Inhibition of hydroxymethylglutaryl-coenzyme A synthase by L-659,699 *Proc Natl Acad Sci U S A*
905 **84**, 7488-7492

906 26. Greenspan, M. D., Bull, H. G., Yudkovitz, J. B., Hanf, D. P., and Alberts, A. W. (1993) Inhibition of
907 3-hydroxy-3-methylglutaryl-CoA synthase and cholesterol biosynthesis by beta-lactone inhibitors
908 and binding of these inhibitors to the enzyme *Biochem J* **289 (Pt 3)**, 889-895

909 27. Tomoda, H., Kumagai, H., Takahashi, Y., Tanaka, Y., Iwai, Y., and Omura, S. (1988) F-244
910 (1233A), a specific inhibitor of 3-hydroxy-3-methylglutaryl coenzyme A synthase: taxonomy of
911 producing strain, fermentation, isolation and biological properties *J Antibiot (Tokyo)* **41**, 247-249

912 28. Tomoda, H., Kumagai, H., Tanaka, H., and Omura, S. (1987) F-244 specifically inhibits 3-hydroxy-
913 3-methylglutaryl coenzyme A synthase *Biochim Biophys Acta* **922**, 351-356

914 29. Tomoda, H., Kumagai, H., Tanaka, H., and Omura, S. (1993) Specific binding of beta-lactone
915 1233A to 3-hydroxy-3-methylglutaryl-coenzyme A synthase *J Antibiot (Tokyo)* **46**, 872-874

916 30. Tomoda, H., Ohbayashi, N., Morikawa, Y., Kumagai, H., and Omura, S. (2004) Binding site for
917 fungal beta-lactone hymeglusin on cytosolic 3-hydroxy-3-methylglutaryl coenzyme A synthase
918 *Biochim Biophys Acta* **1636**, 22-28

919 31. Skaff, D. A., Ramyar, K. X., McWhorter, W. J., Barta, M. L., Geisbrecht, B. V., and Miziorko, H. M.
920 (2012) Biochemical and structural basis for inhibition of Enterococcus faecalis
921 hydroxymethylglutaryl-CoA synthase, mvaS, by hymeglusin *Biochemistry* **51**, 4713-4722

922 32. Shafqat, N., Turnbull, A., Zschocke, J., Oppermann, U., and Yue, W. W. (2010) Crystal structures
923 of human HMG-CoA synthase isoforms provide insights into inherited ketogenesis disorders and
924 inhibitor design *J Mol Biol* **398**, 497-506

925 33. Pojer, F., Ferrer, J. L., Richard, S. B., Nagegowda, D. A., Chye, M. L., Bach, T. J. *et al.* (2006)
926 Structural basis for the design of potent and species-specific inhibitors of 3-hydroxy-3-
927 methylglutaryl CoA synthases *Proc Natl Acad Sci U S A* **103**, 11491-11496

928 34. Trub, A. G., Wagner, G. R., Anderson, K. A., Crown, S. B., Zhang, G. F., Thompson, J. W. *et al.*
929 (2022) Statin therapy inhibits fatty acid synthase via dynamic protein modifications *Nat Commun*
930 **13**, 2542

931 35. Wagner, G. R., Bhatt, D. P., O'Connell, T. M., Thompson, J. W., Dubois, L. G., Backos, D. S. *et al.*
932 (2017) A Class of Reactive Acyl-CoA Species Reveals the Non-enzymatic Origins of Protein
933 Acylation *Cell Metab* **25**, 823-837 e828

934 36. Nabet, B., Ferguson, F. M., Seong, B. K. A., Kuljanin, M., Leggett, A. L., Mohardt, M. L. *et al.* (2020)
935 Rapid and direct control of target protein levels with VHL-recruiting dTAG molecules *Nat Commun*
936 **11**, 4687

937 37. Jo, Y., and DeBose-Boyd, R. A. (2022) Post-Translational Regulation of HMG CoA Reductase *Cold*
938 *Spring Harb Perspect Biol* **14**,

939 38. Medina, M. W., Theusch, E., Naidoo, D., Bauzon, F., Stevens, K., Mangravite, L. M. *et al.* (2012)
940 RHOA is a modulator of the cholesterol-lowering effects of statin *PLoS Genet* **8**, e1003058

941 39. Madison, B. B. (2016) Srebp2: A master regulator of sterol and fatty acid synthesis *J Lipid Res* **57**,
942 333-335

943 40. Pandyra, A., and Penn, L. Z. (2014) Targeting tumor cell metabolism via the mevalonate pathway:
944 Two hits are better than one *Mol Cell Oncol* **1**, e969133

945 41. Clendening, J. W., Pandyra, A., Li, Z., Boutros, P. C., Martirosyan, A., Lehner, R. *et al.* (2010)
946 Exploiting the mevalonate pathway to distinguish statin-sensitive multiple myeloma *Blood* **115**,
947 4787-4797

948 42. Longo, J., Mullen, P. J., Yu, R., van Leeuwen, J. E., Masoomian, M., Woon, D. T. S. *et al.* (2019)
949 An actionable sterol-regulated feedback loop modulates statin sensitivity in prostate cancer *Mol*
950 *Metab* **25**, 119-130

951 43. Ariyasu, S., Hayashi, H., Xing, B., and Chiba, S. (2017) Site-Specific Dual Functionalization of
952 Cysteine Residue in Peptides and Proteins with 2-Azidoacrylates *Bioconjug Chem* **28**, 897-902

953 44. Cistola, D. P., Small, D. M., and Hamilton, J. A. (1987) Carbon 13 NMR studies of saturated fatty
954 acids bound to bovine serum albumin. I. The filling of individual fatty acid binding sites *J Biol Chem*
955 **262**, 10971-10979

956 45. Tomoda, H., Ohbayashi, N., Kumagai, H., Hashizume, H., Sunazuka, T., and Omura, S. (1999)
957 Differential inhibition of HMG-CoA synthase and pancreatic lipase by the specific chiral isomers of
958 beta-lactone DU-6622 *Biochem Biophys Res Commun* **265**, 536-540

959 46. Burslem, G. M., Smith, B. E., Lai, A. C., Jaime-Figueroa, S., McQuaid, D. C., Bondeson, D. P. *et*
960 *al.* (2018) The Advantages of Targeted Protein Degradation Over Inhibition: An RTK Case Study
961 *Cell Chem Biol* **25**, 67-77 e63

962 47. Kiely-Collins, H., Winter, G. E., and Bernardes, G. J. L. (2021) The role of reversible and irreversible
963 covalent chemistry in targeted protein degradation *Cell Chem Biol* **28**, 952-968

964 48. Guo, W. H., Qi, X., Yu, X., Liu, Y., Chung, C. I., Bai, F. *et al.* (2020) Enhancing intracellular
965 accumulation and target engagement of PROTACs with reversible covalent chemistry *Nat Commun*
966 **11**, 4268

967 49. Mishra, V., and Heath, R. J. (2021) Structural and Biochemical Features of Human Serum Albumin
968 Essential for Eukaryotic Cell Culture *Int J Mol Sci* **22**,

969 50. van der Vusse, G. J. (2009) Albumin as fatty acid transporter *Drug Metab Pharmacokinet* **24**, 300-
970 307

971 51. Paulo, J. A., O'Connell, J. D., Everley, R. A., O'Brien, J., Gygi, M. A., and Gygi, S. P. (2016)
972 Quantitative mass spectrometry-based multiplexing compares the abundance of 5000 S. cerevisiae
973 proteins across 10 carbon sources *J Proteomics* **148**, 85-93

974 52. Eng, J. K., Hoopmann, M. R., Jahan, T. A., Egertson, J. D., Noble, W. S., and MacCoss, M. J.
975 (2015) A deeper look into Comet--implementation and features *J Am Soc Mass Spectrom* **26**, 1865-
976 1874

977 53. Eng, J. K., Jahan, T. A., and Hoopmann, M. R. (2013) Comet: an open-source MS/MS sequence
978 database search tool *Proteomics* **13**, 22-24

979 54. Rad, R., Li, J., Mintseris, J., O'Connell, J., Gygi, S. P., and Schweppe, D. K. (2021) Improved
980 Monoisotopic Mass Estimation for Deeper Proteome Coverage *J Proteome Res* **20**, 591-598

981 55. Elias, J. E., and Gygi, S. P. (2007) Target-decoy search strategy for increased confidence in large-
982 scale protein identifications by mass spectrometry *Nat Methods* **4**, 207-214

983 56. Huttlin, E. L., Jedrychowski, M. P., Elias, J. E., Goswami, T., Rad, R., Beausoleil, S. A. *et al.* (2010)
984 A tissue-specific atlas of mouse protein phosphorylation and expression *Cell* **143**, 1174-1189

985 57. Savitski, M. M., Wilhelm, M., Hahne, H., Kuster, B., and Bantscheff, M. (2015) A Scalable Approach
986 for Protein False Discovery Rate Estimation in Large Proteomic Data Sets *Mol Cell Proteomics* **14**,
987 2394-2404

988 58. Beausoleil, S. A., Villen, J., Gerber, S. A., Rush, J., and Gygi, S. P. (2006) A probability-based
989 approach for high-throughput protein phosphorylation analysis and site localization *Nat Biotechnol*
990 **24**, 1285-1292

991 59. Tyanova, S., Temu, T., Sinitcyn, P., Carlson, A., Hein, M. Y., Geiger, T. *et al.* (2016) The Perseus
992 computational platform for comprehensive analysis of (prote)omics data *Nat Methods* **13**, 731-740

993 60. Itzhak, D. N., Tyanova, S., Cox, J., and Borner, G. H. (2016) Global, quantitative and dynamic
994 mapping of protein subcellular localization *Elife* **5**,

995